Molecular Therapy
Original Article

Preclinical efficacy and safety assessment of engineered regulatory T cells for treatment of IPEX and other autoimmune disorders

Yuchi Honaker,[1] Noelle P. Dahl,[1] Swati Singh,[1] Akhilesh K. Singh,[1] Christina Lopez,[1] David Gruber,[1] Samuel C. Scharffenberger,[1] Shivani Patel,[1] Harold Jones,[1] Iram F. Khan,[1] Michelle L. Christian,[1] Su Jung Yang,[1] Karen Sommer,[1] Troy R. Torgerson,[1,2] Eric J. Allenspach,[1,2] Cade Ellis K. Ito,[3] Gene I. Uenishi,[3] Gregory J. Cost,[3] Peter J. Cook,[1] and David J. Rawlings[1,2,4]

[1]Center for Immunity and Immunotherapies and Program for Cell and Gene Therapy, Seattle Children's Research Institute, Seattle, WA 98101, USA; [2]Department of Pediatrics, University of Washington School of Medicine, Seattle, WA 98105, USA; [3]Casebia Therapeutics, Cambridge, MA 02139, USA; [4]Department of Immunology, University of Washington School of Medicine, Seattle, WA 98109, USA

FOXP3 is an essential transcription factor driving lineage commitment and function of regulatory T cells (Tregs). We previously reported a proof-of-concept study describing engineered Tregs (EngTregs) generated using homology-directed repair-based editing of the *FOXP3* gene in CD4$^+$ T cells, resulting in constitutive, high-level endogenous FOXP3 expression leading to acquisition of a Treg phenotype and robust *in vitro* and *in vivo* suppressive function. Here, we expand this gene-editing strategy to integrate a functional FOXP3 cDNA to enable EngTreg therapy for immune dysregulation, poly-endocrinopathy, enteropathy, X-linked syndrome (IPEX), a devastating multiorgan autoimmune disorder mediated by mutations within the *FOXP3* gene. We provide a detailed characterization of preclinical EngTreg generation, including gene targeting efficiencies, cell enrichment and expansion, analyses of potential off-target editing, and phenotypic and functional characterization, including *in vitro* suppression of effector T cells and *in vivo* reversal of graft-versus-host disease. Importantly, in parallel, we utilize syngeneic and humanized mouse models to demonstrate the safety of EngTregs in primary and secondary humoral responses and viral infection control, respectively. Our combined preclinical dataset strongly supports the efficacy and safety of EngTregs as a promising potential cellular therapeutic approach for IPEX and possibly other autoimmune disorders.

INTRODUCTION

Regulatory T cells, or Tregs, comprise a relatively rare subset of CD4$^+$ T cells in peripheral blood (PB) and tissues that mediate a critical role in the maintenance of immune tolerance and control autoreactive immune responses. Based on their robust immunosuppressive features, Treg-based cell therapies are being explored as potential treatments to ameliorate autoimmune diseases and improve the clinical outcomes of hematopoietic stem cell and solid organ transplantation.[1–4] However, because Tregs represent only a small fraction of peripheral immune cells and lack specific surface markers, one major hurdle in adoptive Treg cell therapy is isolation and expansion of Tregs to achieve the required cell purity and dose for therapeutic application.

FOXP3 is the master transcription factor governing Treg lineage development, maintenance, and function. Based upon this concept, we previously developed a FOXP3 gene-editing strategy to generate engineered Tregs (EngTregs) from bulk CD4$^+$ T cells.[5] This approach utilized site-specific homology-directed repair (HDR) to integrate a constitutively active MND promoter into the *FOXP3* locus, thus bypassing endogenous epigenetic and transcriptional inhibition of the *FOXP3* promoter in conventional CD4$^+$ T cells. HDR integration of the MND promoter at the *FOXP3* locus promotes stable FOXP3 expression in the resulting products and reduces the risk of silencing and instability. The introduction of stable, high-level expression of FOXP3 resulted in EngTregs exhibiting a Treg-like immunophenotype and robust *in vitro* and *in vivo* suppressive function comparable to that of thymic Treg (tTreg).[5] EngTregs generated with this approach and additional technical modifications[5–9] provide potential manufacturing and stability benefits in comparison with conventional Treg enrichment strategies, and significant potential as a cell therapy for autoimmune diseases and graft-versus-host disease (GvHD).

The crucial role for FOXP3 in human immune tolerance was first identified in the primary immune dysregulation disorder, IPEX (immune dysregulation, poly-endocrinopathy, enteropathy, X-linked syndrome), resulting from loss-of-function mutations

Received 27 June 2025; accepted 9 March 2026;
https://doi.org/10.1016/j.ymthe.2026.03.017.

Correspondence: David J. Rawlings, Center for Immunity and Immunotherapies and Program for Cell and Gene Therapy, Seattle Children's Research Institute, Seattle, WA 98101, USA.
E-mail: drawling@uw.edu

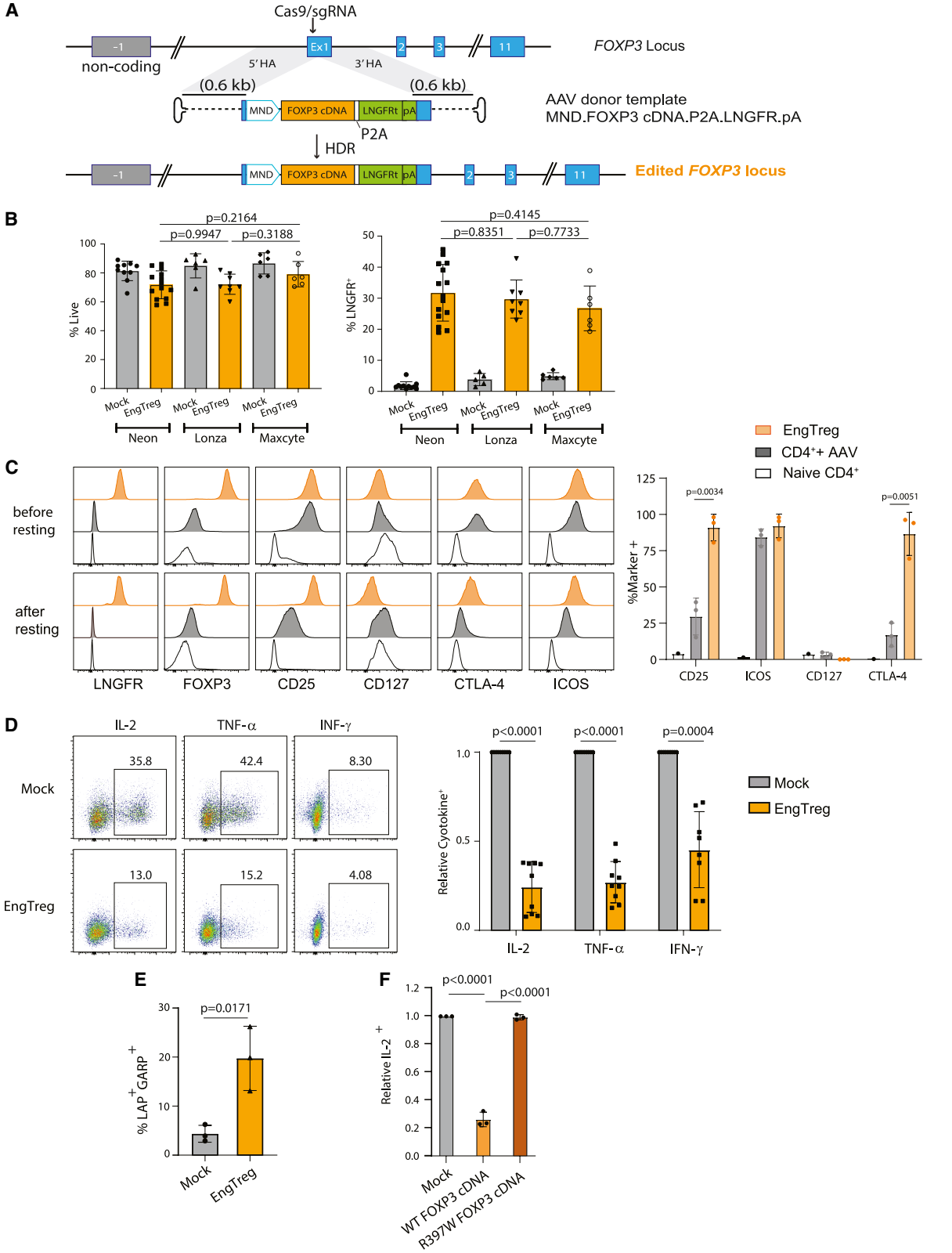

(legend on next page)

within the *FOXP3* locus.[10–12] These monogenic *FOXP3* mutations disrupt normal Treg development and result in excessive immune responses to autoantigens, dysregulated lymphocyte activation, and early onset multi-organ autoimmune disease.[13,14] Affected males typically develop systematic autoimmunity shortly after birth, with clinical characteristics that include severe enteropathy, type 1 diabetes, thyroiditis, and dermatitis—features that are often poorly responsive to immunosuppressive therapy. The current standard of care includes aggressive immunosuppression followed by allogenic hematopoietic stem cell transplantation (HSCT).[15] Without intervention, most patients exhibit early mortality, often succumbing within the first 2 years of life. As HSCT is limited by donor availability and post-transplant morbidity, and outcomes are impacted by the pre-transplant response to immunosuppression and ongoing organ damage, the development of novel treatment strategies for IPEX is urgently needed.

Reversion mosaicism in primary immunodeficiencies, including IPEX, suggest that genetic restoration of key gene function has the potential to mitigate disease.[16–18] However, our previous HDR-based FOXP3 editing strategy for EngTreg is not applicable to patients with loss-of-function mutations within the FOXP3 locus. Therefore, in this study, we aimed to advance an EngTreg strategy for direct application to IPEX patients and to comprehensively address key preclinical questions relevant to both potential efficacy and safety. Here, we describe an EngTreg strategy using $CD4^+$ T cells isolated from IPEX (or healthy donor) subjects. Modifying our original method using CRISPR-Cas9 and HDR, we incorporated a FOXP3 cDNA expression cassette within a modified adeno-associated virus (AAV) homology donor template designed to disrupt and replace endogenous FOXP3 transcripts upon HDR. Importantly, EngTregs generated from PB $CD4^+$ T cells of IPEX patients resembled those derived from healthy donors exhibiting robust FOXP3 cDNA expression, Treg-like immunophenotype and function, and a broad T cell receptor (TCR) repertoire potentially capable of capturing specificities present in expanded pathogenic $CD4^+$ effector T cells (Teff). EngTregs were efficiently generated from healthy donor $CD4^+$ T cells isolated from leukapheresis, PB, or cord blood (CB). Furthermore, we demonstrate both the efficacy and safety of EngTregs in a range of preclinical animal models. Overall, our extensive non-clinical dataset demonstrates the manufacturing feasibility, suppressive function, and safety of the EngTregs, suggesting a promising stand-alone, or as bridge to transplant, adoptive Treg cell therapy for IPEX.

RESULTS

EngTreg generation via HDR-based delivery of a FOXP3 cDNA expression cassette

Because IPEX-associated mutations occur across the entire *FOXP3* gene,[19,20] we designed an HDR-based gene-editing approach to simultaneously disrupt expression of the mutant, endogenous FOXP3 protein and introduce a functional FOXP3 cDNA sequence using an optimized HDR donor template. Several single-guide RNAs (sgRNAs) targeting the first coding exon of *FOXP3* were evaluated for their on-target cutting efficiency (Figures S1A and S1B). The T9 gRNA was chosen for subsequent HDR gene editing based on high insertion or deletion (indel) score and proximity to the transcription start site. Electroporation of Cas9/T9 sgRNA ribonucleoprotein (RNP) complex into activated $CD4^+$ T cells resulted in an average of 90% non-homologous end joining (NHEJ)-mediated indels at the *FOXP3* locus. Predicted off-target sites for the T9 guide were evaluated, with none of the top six showing significant levels in indel induction in primary human T cells (Figures S1C and S1D). We subsequently performed an unbiased, genome-wide off-target analysis, comparing research versus Good Manufacturing Practices (GMP) grade Cas9 and sgRNA. As expected, GMP grade reagents reduced indels across all candidates' off-target sites while maintaining high on-target cutting efficiency (Figures S1E and S1F).

Sequences spanning 0.6 kb immediately upstream and downstream of the T9 cut site were cloned into the AAV template as the left (5′) and right (3′) homology arms (HAs), respectively. An expression cassette consisting of MND promoter FOXP3 cDNA, P2A ribosomal skipping sequence, intracellularly truncated LNGFR (LNGFRt), and SV40 poly(A) was subsequently cloned within the HAs (Figure 1A). To optimize HDR rates, we evaluated

Figure 1. Generation of EngTregs expressing MND-driven *FOXP3* cDNA and LNGFRt surface marker

(A) Illustration of homology-directed repair (HDR)-mediated *FOXP3* editing. Top: gRNA targets the first coding exon of human *FOXP3*. Center: AAV donor template contains an expression cassette flanked by 0.6 kb *FOXP3* homology arm (HA) sequences upstream and downstream of the Cas9-gRNA cut site. The expression cassette consists of an MND promoter, coding sequences of human *FOXP3* cDNA, P2A ribosome skipping peptide, truncated LNGFR, and the SV40 poly(A) sequences. Bottom: HDR results in an edited *FOXP3* allele with the integrated expression cassette and disrupted endogenous *FOXP3* gene expression. (B) Graphs of cell viability (left) and HDR efficiency (right) on day 2 following transfection (using Neon, Lonza 4D, or Maxcyte instruments) and subsequent AAV transduction. Percent live cells were gated as viability dye-negative in total samples (left); percent $LNGFR^+$ cells were gated in live single $CD4^+$ cells (right). Data were graphed as mean ± SD, n = 10, 8, and 6 for Neon, Lonza 4D, and Maxcyte, respectively, from 5–6 healthy donors. (C) Immunophenotype characterization of EngTreg products. (Left) Histograms of indicated markers stained immediately after thawing the cell product ("before resting") or after a 3-day culture in low IL-2 ("after resting"). (Right) Graphs of marker positivity in rested condition for three independent EngTreg donor products. Naive $CD4^+$ T cells (shown as control) were isolated from bulk $CD4^+$ cells not previously cultured or activated by CD3/CD28 beads. Mock-edited and EngTregs were cryopreserved after EngTreg production using two rounds of CD3/CD28 beads stimulation, once before editing and once during post-editing cell expansion. (D) Mock-edited or EngTregs were treated with PMA and ionomycin in the presence of GolgiStop for 5 h before assessing intracellular cytokine positivity. Flow plots are representative results gated on $CD4^+$ cells. Relative cytokine positivity compared to mock-edited cells was graphed as mean ± SD from 7 experiments. (E) Surface expression of LAP and GARP in mock-edited and EngTreg cells in response to activation. LAP^+GARP^+ was gated on $CD4^+$ T cells. n = 3; a two-tailed t test was performed to obtain p value. (F) IL-2 positivity in mock-edited or edited cells expressing wild-type (WT) or R397W FOXP3 cDNA upon PMA/ionomycin stimulation. Graph shows mean ± SD compared to mock-edited cells; n = 3. p value by one-way ANOVA.

potential options for larger-scale gene editing and manufacturing, including comparing alternative electroporation systems. As shown in Figure 1B, comparable post-editing cell viability was observed across Neon,[21] Lonza, and Maxcyte electroporation systems. In mock-edited cells, which were electroporated with Cas9 alone and transduced with AAV, approximately 80% of cells were viable 2 days post-editing. EngTregs electroporated with Cas9/sgRNA RNP and immediately transduced with AAV displayed similar cell viability and HDR editing rates (as measured by the expression of LNGFR and FOXP3) across electroporation platforms (Figures 1B and 1C). Of note, we also compared LNGFR and FOXP3 expression in EngTregs expressing FOXP3cDNA versus endogenous FOXP3 (LNGFR.P2A knockin EngTreg) described in the previous studies, both driven by an exogenous MND promoter.[5,6] While both methods yielded similar levels of *cis*-linked LNGFR expression, MND-driven FOXP3 cDNA-edited cells exhibited slightly lower FOXP3 levels (based upon mean fluorescence intensity) than the MND-driven endogenous FOXP3 expression (Figure S2A). This difference may be explained by the absence of intron 1-residing CNS3 regulatory elements in the FOXP3 cDNA sequences.

FOXP3cDNA EngTregs were analyzed for expression of the Treg-associated markers, including CD25, CD127, CTLA-4, and ICOS (Figure 1C). At the time of cryopreservation, both $CD4^+$ T cell control and FOXP3cDNA EngTregs were activated following expansion; therefore, thawed mock-edited $CD4^+$ T cells showed activation-dependent expression of these markers compared with non-expanded naive $CD4^+$ cells. Following thaw and a period of rest in culture, only EngTregs exhibited high levels of CD25, CTLA-4, and ICOS and reduction of CD127 consistent with a Treg phenotype. Upon stimulation, EngTregs produced fewer proinflammatory cytokines (Figure 1D) and displayed enhanced surface expression of the transforming growth factor β (TGF-β)-associated factors LAP and GARP (Figure 1E), features also consistent with a Treg-like phenotype. Conversely, EngTregs expressing a loss-of-function R397W FOXP3 cDNA failed to reduce interleukin-2 (IL-2) production (Figure 1F) or upregulate CD25 and CTLA-4 (Figure S2B), indicating that functional FOXP3 is required to induce Treg-like properties in conventional $CD4^+$ T cells.

Next, we developed a GMP-like process to generate preclinical EngTreg cell products (Figure 2A). On day 0, isolated $CD4^+$ T cells were activated with anti-CD3/CD28 beads and IL-2 for 72 h. After bead removal on day 3, cells were cultured overnight (∼18 h) before proceeding to gene editing on day 4. An average 4.5-fold expansion in cell numbers was observed between activation bead addition and gene editing. Electroporated cells were plated and immediately transduced with AAV at 20% of culture volume. Approximately 24 h later, cell culture volume was doubled to dilute AAV. On day 7, LNGFR expression was evaluated by flow cytometry, followed by column-based enrichment using anti-LNGFR antibody affinity microbeads, as previously described.[5] Between day 4 (gene editing) and day 7 (enrichment), a 3- to 4-fold change in cell numbers was observed. As shown in Figure 2B, $LNGFR^{low}$ cells resulting from episomal AAV expression were present in both mock-treated cells and EngTreg prior to enrichment, while $LNGFR^{high}$ -expressing populations were only detected in cells receiving Cas9/gRNA and AAV, consistent with HDR-mediated cassette integration. LNGFR-enriched EngTreg yielded a highly pure $LNGFR^{high}$ population (90.4%–99.5% $LNGFR^+$ across 5 studies). Enriched EngTregs were next expanded in G-Rex flasks with anti-CD3/CD28 beads (3:1 bead-to-cell ratio) in culture media supplemented with 100 ng/mL IL-2 and 100 nM rapamycin. On the 3^{rd} and 5^{th} days of G-Rex expansion, the half-volume of culture media was replaced with fresh media containing 100 ng/mL IL-2. EngTregs were harvested after a 7-day G-Rex expansion (day 14 in process described in Figure 2A). The resulting cell products maintained high LNGFR expression (Figures 2B and 2C) and were cryopreserved following bead removal. On average, seeding 4×10^7 enriched EngTreg cells in G-Rex flasks yielded 2×10^9 cells (∼50-fold expansion) (Figure 2D).

Molecular analyses were performed on EngTregs harvested on day 14 to confirm on-target and seamless HDR donor template integration. Percent integration as determined by droplet digital PCR (ddPCR; using amplicons capturing LNGFR and downstream of the 3′ HA) correlated closely with LNGFR expression as measured by flow cytometry (Figures 2C and 2E). PCR using primers outside of the 5′ and 3′ HAs also resulted in the expected amplicon containing donor template integration (Figure 2E, right) and sequencing validated seamless integration of the donor template at the CRISPR cut site (Figure S3). TCR repertoire analysis of EngTregs demonstrated sustained clonal diversity during the process of *in vitro* cell engineering and expansion (Figure S4).

Functional assessment of EngTregs expressing FOXP3 cDNA

We first assessed the function of FOXP3 cDNA expressing EngTregs using an *in vitro* suppression assay wherein the level of $CD4^+$ T cell proliferation was monitored in response to anti-CD3/CD28-mediated activation (Figure 3A). Autologous EngTreg expressing FOXP3 cDNA effectively suppressed $CD4^+$ T cell proliferation (Figure 3B), with activity levels equivalent to control, *ex vivo* expanded tTregs. Of note, consistent with tTreg proliferative activity, both EngTregs and tTregs exhibited similar, attenuated proliferation relative to mock-edited T cells (Figure S5). To directly assess *in vivo* function, we next evaluated EngTregs in a xenoGvHD model. As previously described,[5] adoptive transfer of Tregs in this model can suppress xenoGvHD disease onset and reduce overall disease severity. As outlined schematically in Figure 3C, cryopreserved unedited tTreg, EngTreg, or mock-edited CD4+ control human cell products were thawed and transferred intravenously (I.V.) into irradiated NSG recipient mice 3 days prior to infusion of autologous $CD4^+$ T cells. Pre-treatment with EngTreg expressing FOXP3 cDNA delayed disease onset and significantly increased survival rate (Figure 3D), with results equivalent to control tTreg-treated mice. Mice that received either EngTreg or tTreg had significantly lower GvHD scores and improved body weight compared with mice receiving sham- or mock-edited $CD4^+$ T cells (Figure 3E).

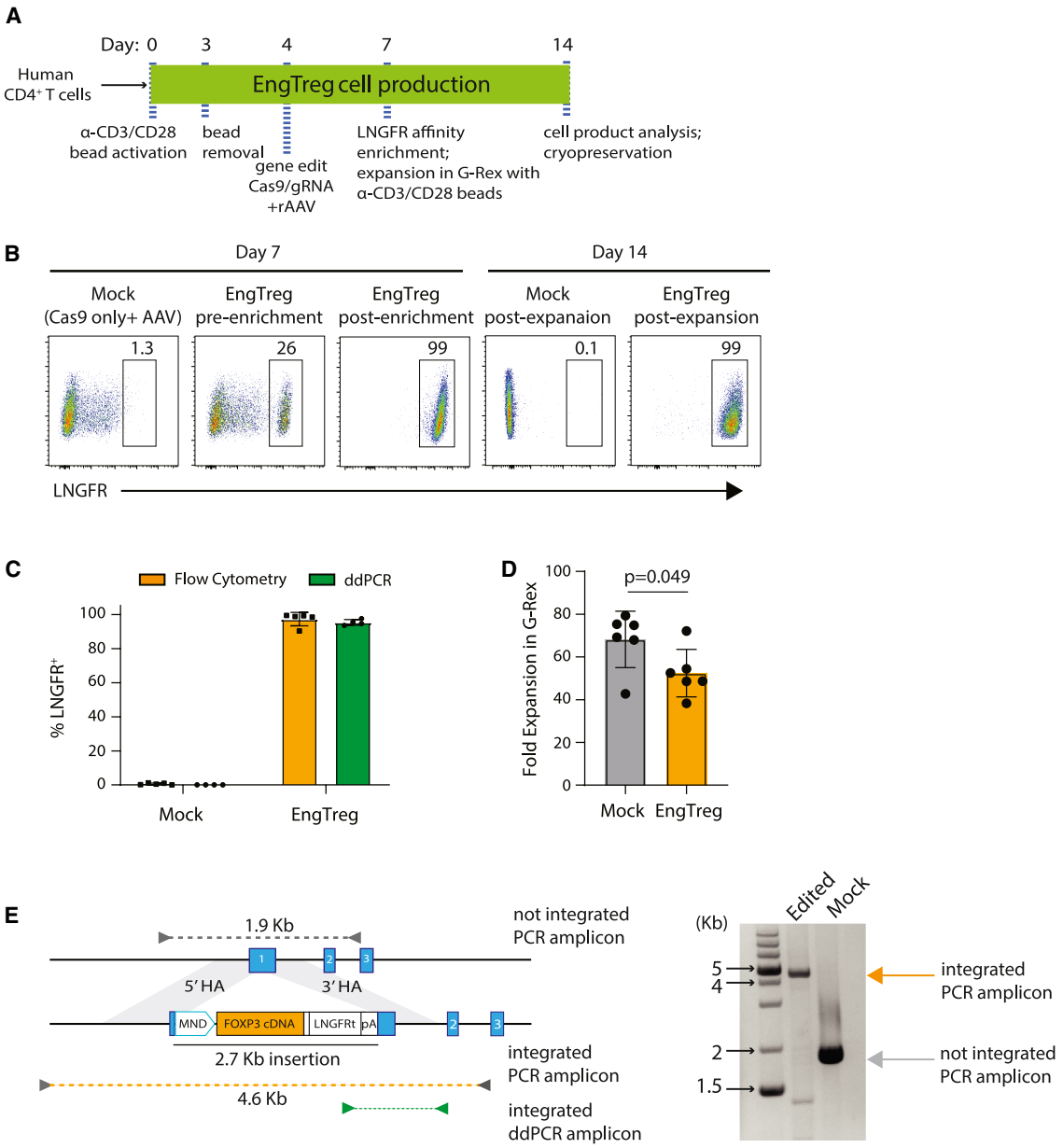

Figure 2. Generation of preclinical grade EngTregs

(A) Schematic illustrates the major steps in the EngTreg production process. (B) Representative flow plots show percent LNGFR$^+$ before and after the LNGFR-mediated affinity enrichment (at day 7) and after expansion in G-Rex (day 14). Cells were gated on live singlet CD4$^+$ T cells. Low levels of LNGFR expression observed in both edited and mock-edited cells 3 days after AAV transduction due to episomal AAV expression were not enriched by LNGFR affinity selection. (C) Graph (mean ± SD) of day 14 cell product purity determined by flow cytometry (n = 6 from six healthy donors) and ddPCR. For ddPCR, percent LNGFR$^+$ was calculated as the ratio of the LNGFR$^+$ concentration to the reference control concentration (n = 4 from four healthy donors). (D) Graph (mean ± SD) of fold increase in cell numbers on day 14 following expansion in G-Rex (n = 6 from six healthy donors). (E) Diagram illustrates the PCR and ddPCR detection of repair template integration. The gray triangles indicate the oligo pairs used in PCR reactions targeting sequences outside of the HAs. The resulting 1.9- and 4.2-kb amplicons with or without integrated expression cassette are shown in gray and orange dashed lines, respectively. The green triangles and dashed line indicate the oligo pairs and amplicon in ddPCR reactions. The gel image shown at right contains PCR products amplified from genomic DNA of EngTregs or mock-edited cell products.

Based on the assays performed, EngTreg products expressing the FOXP3 cDNA exhibited *in vitro* and *in vivo* suppressive function equivalent to control tTreg populations.

Because IPEX patients (as well as subjects undergoing solid organ transplant or HSCT) are frequently treated with immunosuppressants, we next determined whether EngTregs can retain activity in

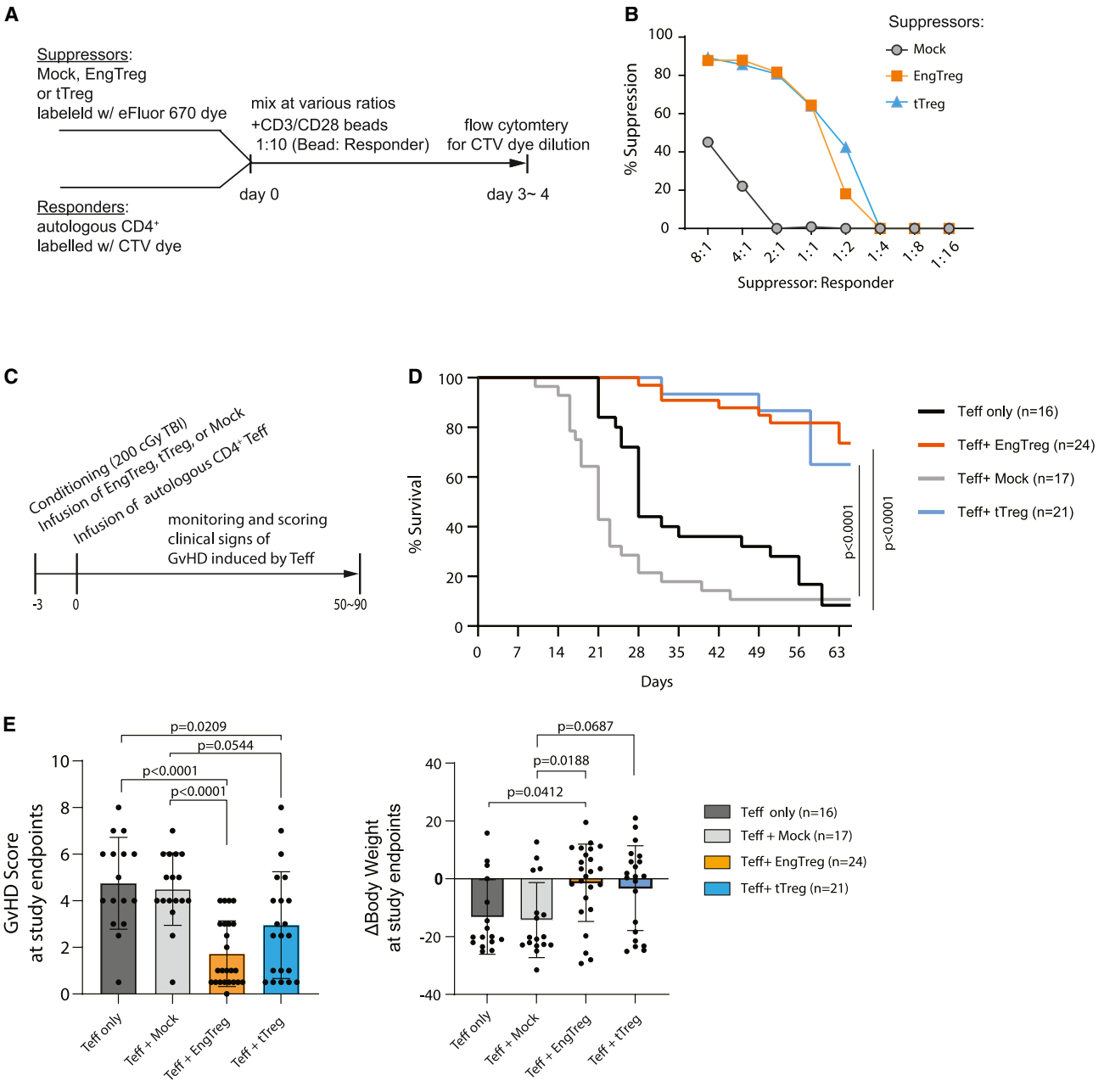

Figure 3. EngTreg with FOXP3 cDNA expression exhibit suppressive function *in vitro* and *in vivo*

(A) Schematic of *in vitro* suppression assay. (B) Graph of representative data (n = 4) showing suppression of CD3/CD28-bead stimulated responder cell proliferation at the indicated suppressor-to-responder ratios. Percent suppression = ([% divided with no Treg − % divided with Treg]/% divided with no Treg) × 100. (C) Schematic of *in vivo* suppression in CD4$^+$ adoptive transfer xenogeneic GvHD. Minimally irradiated NSG mice were assigned to one of the four cohorts shown, receiving freshly thawed human CD4$^+$ T cells from PBMCs (Teff) with or without autologous EngTreg, tTreg, or mock-edited cells. (D) Survival curve from three studies combined, with total animal numbers indicated in the key. p values from log rank (Mantel-Cox) test. (E) Graphs (mean ± SEM) show the GvHD scores (left) and body weight changes (right) at study endpoints combined from three independent studies. p values from one-way ANOVA with Tukey's multiple comparisons test.

the presence of alternative, clinically relevant, immunosuppressant drugs *in vitro* (Figure 4A). To this end, cell expansion and viability were evaluated after culturing EngTreg or mock-edited cells in the presence of rapamycin, everolimus, tacrolimus, or prednisone (Figures 4B and 4C). EngTreg, in contrast to mock-edited CD4$^+$ T cells, remained viable and proliferative in response to TCR activation in the presence of all candidate drugs, across a broad range of therapeutic doses.[22–26]

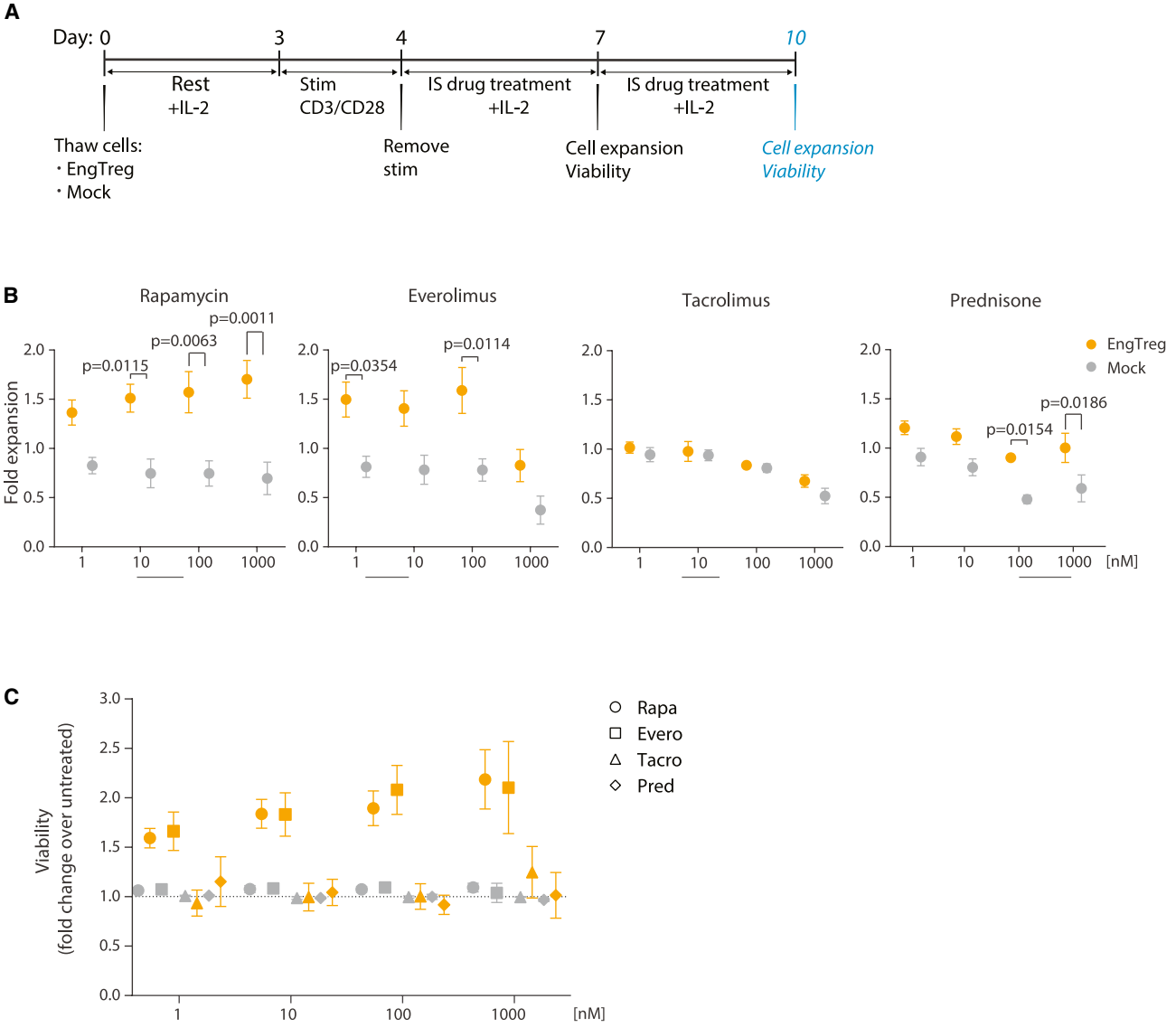

Figure 4. Minimal impact of immunosuppression drugs on EngTregs

(A) Schematic showing the experimental timeline for *in vitro* immunosuppressive drug response assay. (B) Combined growth data for mock and EngTreg in the presence of immunosuppressive drugs over the indicated dose range at day 10 from three independent experiments. Shown as fold change relative to untreated group for mock or EngTregs, respectively, with the gray bars (on *x* axis) denoting approximate clinical dose range. Data shown as mean ± SD, *p* values calculated by a two-way ANOVA with Sidak's multiple comparison test. (C) Combined viability of mock or EngTregs as fold change compared with relevant untreated groups over drug dose range, from three independent experiments. Data shown as mean ± SD.

Generation EngTreg from umbilical CB

Umbilical CB represents an alternative attractive source to develop cell therapies beyond HSCT.[27,28] The potential advantages of CB-derived T cell therapies over products derived from PB include a higher percentage of naive cells, broader clonal diversity, reduced differentiation and exhaustion phenotypes, potential for longer persistence, and enhanced tolerance to HLA mismatch. Thus, we explored the feasibility of generating EngTregs from CB-derived $CD4^+$ T cells based on the EngTreg production protocol described in Figure 2A. We observed comparable cell expansion between PB- and CB-derived $CD4^+$ T cells in response to CD3/CD28-dependent activation prior to editing (Figure S6A). Editing efficiency, LNGFRt-mediated enrichment, and high LNGFR purity after expansion was also achieved in CB-derived $CD4^+$ T cells (Figures S6B and S6C; data not shown). Interestingly, a reduction in cell viability (data not shown) and fold expansion (Figure S6D) was observed at the end of the expansion in CB-derived EngTreg compared to PB-derived EngTreg. An alternative, optimized protocol, specific for

CB-derived EngTreg, was developed that improved yields and viability during expansion with culture media containing a lower dose of IL-2 (50 ng/mL) (Figures S6E and S6F). Functionally, CB-derived EngTregs exhibited a Treg-like immunophenotype and reduced the production of proinflammatory cytokines compared with mock-edited $CD4^+$ T control cells (Figures S6G and S6H). Importantly, CB-derived EngTregs effectively suppressed allogeneic PB-derived $CD4^+$ T cells in the xenoGvHD model (Figure S6I). The level of protection by CB-derived EngTreg was comparable to autologous PB-derived EngTregs. These data indicated that CB could be used as a source material to generate EngTregs and that such products might be efficacious in the allogeneic setting.

Safety assessment of EngTregs in humoral responses or in response to viral infection

A potential risk for Treg-based cell therapies is non-specific suppression, including blunting of protective immune responses against pathogens. To investigate the potential impact of EngTregs on T-dependent (TD) antibody responses, we utilized adoptive transfer of murine surrogate EngTregs and immunization of immunocompetent recipient mice. Specifically, we evaluated the impact of EngTregs on the response to immunization with NP-CGG conjugate (4-hydroxy-3-nitrophenylacetyl-chicken gamma globulin), a well-characterized TD antigen that induces a robust antibody response, that can be abrogated by $CD4^+$ T cell-depleting monoclonal antibodies.

To test whether EngTregs impede the humoral immune response in this model, we generated murine EngTregs using $CD4^+$ T cells isolated from CD45.1 B6 mice following previously established protocols.[5,6] CRISPR-based HDR at the mouse *Foxp3* locus generated $LNGFR^+$ murine EngTreg that could be enriched and displayed immunosuppressive activity *in vitro* (Figures S7A–S7D). Murine EngTregs (or mock-edited $CD4^+$ T cells or PBS control) were transferred into recipient CD45.2 B6 mice via tail vein (at 2×10^7 cells/kg) 1 day prior to NP-CGG immunization (Figure 5A). A subset of mice from each group was sacrificed at day 0 to verify the homing of $CD45.1^+$ EngTregs to the spleen. As shown in Figures 5A and 5B similar proportions of $CD45.1^+$ donor cells were present in the spleens of mice infused with EngTregs or mock control T cells at day 0, and the majority of infused EngTreg cells retained LNGFR expression. Primary antibody responses (total immunoglobulin G [IgG] and NP-CGG-specific IgG) were measured 9 days post-primary immunization. Next, mice were re-challenged with NP-CGG without adjuvant at day 28, and recall responses were measured on day 42. Animals receiving EngTregs exhibited primary and recall, total, and antigen-specific (NP4) IgG levels comparable to recipients of mock-edited control cells or PBS (Figures 5C and 5D). To confirm the dependence of the NP-CGG antibody response on $CD4^+$ T cells, B6 mice were dosed with an anti-mouse CD4-depleting antibody both before and after immunization (Figure S8A). Mice treated with the depleting antibody showed no induction of mouse IgG in response to immunization relative to mice receiving an isotype control antibody (Figure S8B). These findings demonstrate that humoral immune responses, which are dependent $CD4^+$ T cell help, are not impacted by presence of EngTreg in this model, suggesting that antibody-dependent protective immunity to invading pathogens is unlikely to be negatively impacted in EngTreg-treated patients.

Tregs are selected during thymic development to preferentially suppress autoreactive immune responses rather than responses to foreign pathogens. Thus, we wondered whether autologous EngTreg generated from a pool of $CD4^+$ T cells might contain TCR specificities against previously encountered pathogens/vaccines that might negatively influence immune recall. To address this question, we immunized CD45.1 donor mice with NP-CGG and generated EngTregs from $CD4^+$ T cells isolated 28 days post-immunization (Figure 6A). Using this approach, the $CD4^+$ T cell pool and derived EngTregs were anticipated to contain an enriched population expressing NP-CGG-specific TCRs, expanded in response to the prior immunization. We infused these $CD45.1^+$ EngTregs (2×10^7/kg) or mock-edited cells into CD45.2 recipient mice that had been pre-immunized with NP-CGG 25 days prior to EngTreg/mock injection. Three days later, a subset of mice was euthanized to verify EngTreg and mock-edited cell engraftment and persistence in the spleen (Figure 6B, left). All remaining mice received secondary NP-CGG immunization, and recall responses were assessed on day 42. $LNGFR^+$ EngTreg cells were still detectable in the spleen at this time point (Figure 6B, right). Notably, animals receiving EngTregs exhibited comparable recall total IgG and high affinity NP-CGG-specific IgG responses in comparison to recipients of mock-edited T cells or PBS control (Figures 6C and 6D). Thus, EngTregs generated from NP-CGG antigen-experienced mice did not impact the host humoral immune response. Finally, to compare the potential impact of EngTregs to the immunosuppressant drug rapamycin (modeling, in part, the immunosuppressive environment in IPEX subjects), an additional cohort of immunized animals were treated with rapamycin or vehicle beginning on day 25 of the study (Figure S8C). Rapamycin was administered to maintain clinically relevant trough levels (~10 nM) through the day 42 study endpoint, and recall IgG levels were measured. In contrast to the transfer of EngTregs, rapamycin treatment completely abrogated the IgG recall responses in this setting (Figures 6C and 6D).

Next, we assessed whether human EngTreg impacted viral control in response to Epstein-Barr virus (EBV) infection in a humanized mouse model.[29] In this model, NSG mice were engrafted with human $CD34^+$ PB hematopoietic stem and progenitor cells (HSPCs), followed by EBV challenge at 13 weeks after human cell transfer. Depletion of human $CD4^+$ and $CD8^+$ T cells after viral challenge in this model resulted in an increase in viral load and reduced survival (Figures S9A–S9D), demonstrating that T cells are required to control EBV viral load. As shown schematically in Figure 7A, autologous tTregs and EngTregs were generated and adoptively transferred into recipient mice (2×10^6/kg) following $CD34^+$ HSC engraftment and EBV challenge. Following Treg infusion, EBV viremia was monitored weekly for 3 weeks, and spleens were collected at the experimental endpoint for assessment of viral load and flow cytometry analyses for human immune cell subsets. As shown in Figures 7B–7D and S10A and S10B, EBV-infected mice exhibited a proportional

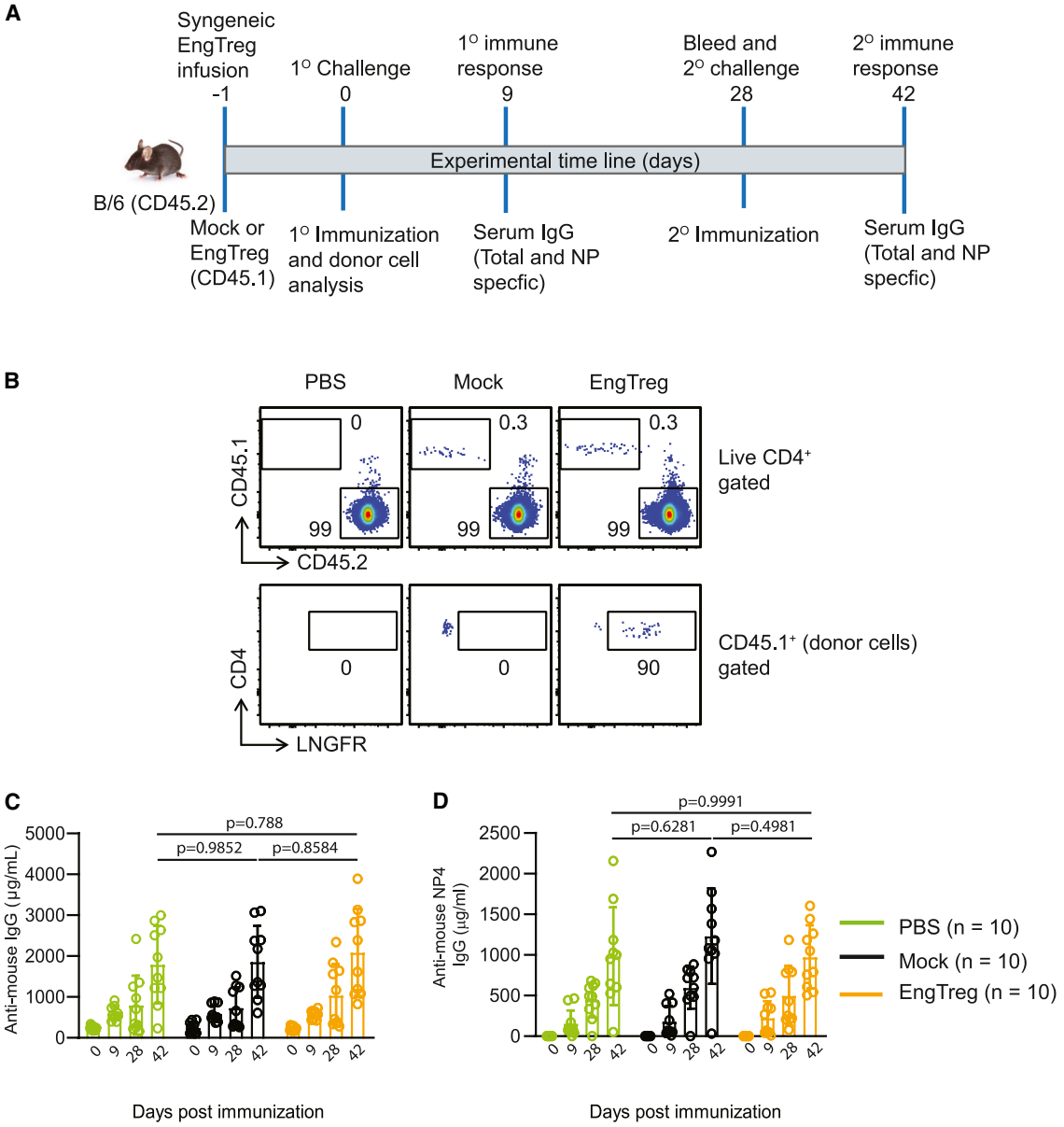

Figure 5. EngTreg do not hinder the host T-dependent humoral response in mouse models

(A) Schematic showing the experimental timeline for NP-CGG-driven antibody response in the presence of syngeneic EngTreg. The 8- to 12-week-old WT (B6) mice received syngeneic mock or EngTreg cells (2×10^7 cells/kg) on day −1 followed by immunization with NP-CGG emulsion on days 0 and 28. (B) Representative flow plots (from two independent experiments) showing the presence of donor CD45.1$^+$ (top) and LNGFR$^+$ (bottom) cells in the spleen of a subset of mice at the time of immunization. (C) Graph showing the serum titer of total IgG at 0, 9, 28, and 42 days post-primary immunization in the presence of the indicated transferred cell populations. Data are combined from two independent experiments and shown as mean ± SD; *p* values calculated using *t* test comparing the IgG antibody titers at day 42. (D) Graph showing the high-affinity (NP-4) NP-specific IgG serum titer at 0, 9, 28, and 42 days post-immunization in the presence of the indicated transferred cell populations. Data are combined from two independent experiments and shown as mean ± SD; *p* values calculated using *t* test comparing the IgG antibody titer at day 42.

increase in total CD45$^+$ human cells, with a reduced proportion of CD19$^+$ B cells, and a marked increase in CD3$^+$ T cells, with a proportional increase in CD8$^+$ T cells accounting for this change. Proportional levels of FOXP3$^+$ cells did not vary in response to EBV infection (Figure S10C). Engrafted LNGFR$^+$ EngTreg were present at sacrifice in recipients of EngTregs. Viral driven alterations in human lymphocyte populations were not impacted by tTreg or EngTreg transfer. The expanded CD8$^+$ T cell pool displayed increased expression of activation markers CD137 and CD69 in EBV-infected groups regardless of the Treg infusion (Figures S9E

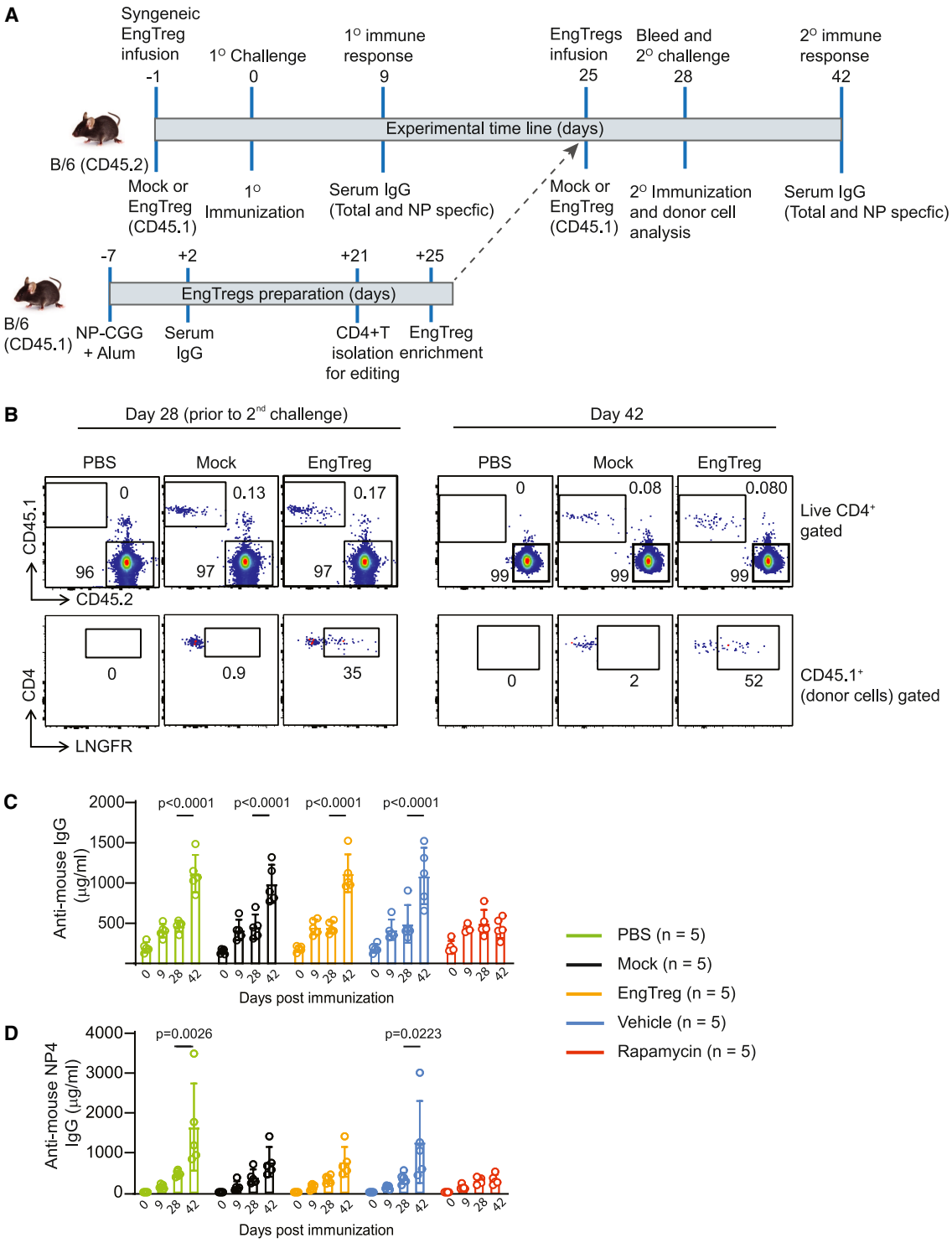

Figure 6. EngTreg generated from a CD4⁺ Teff pool containing NP-specific memory cells does not hinder the host T-dependent humoral memory response

(A) Schematic showing the experimental timeline for NP-CGG-driven memory antibody response in the presence of syngeneic EngTreg generated from the pool of NP antigen-experienced CD4⁺ Teff cells. (B) Representative flow plots showing the presence of donor CD45.1⁺ (top) and LNGFR⁺ (bottom) cells in the spleen of a subset of mice

(legend continued on next page)

and S9F). Similarly, the surface phenotype of the altered human CD19$^+$ B cell compartment (observed in response to EBV infection) was not impacted by Treg infusion (Figures S9E–S9G). Notably, analysis of spleen or blood showed that infusion of tTregs or EngTregs resulted in a similar (or lower) viral load compared with EBV infection alone (Figure 7E). Similarly, overall survival was not impacted by tTreg or EngTreg transfer (Figure 7F). These results demonstrate that EngTreg infusion did not impede the protective T cell immune response modulating viral infection in this humanized EBV infection model.

Efficient generation of FOXP3 cDNA EngTreg from IPEX patient-derived CD4$^+$ T cells

Following demonstration of the suppressive function and safety of EngTregs generated from healthy donors, we next evaluated EngTreg generation using cryopreserved PB mononuclear cells (PBMCs) from five IPEX patients with a range of *FOXP3* mutations. Due to limited cell numbers, we utilized a modified engineering protocol shown schematically in Figure 8A; edited cells were expanded for 3 additional days prior to LNGFR affinity enrichment, followed by 7-day G-Rex expansion. We observed comparable or higher editing efficiency using IPEX subject- versus healthy donor-derived CD4$^+$ T cells (Figure 8B). Prior to cryopreservation, IPEX patient-derived and healthy donor-derived EngTregs displayed equivalent LNGFR purity (>90%; Figure 8C). HDR-mediated expression of FOXP3 cDNA in IPEX patient-derived CD4$^+$ T cells resulted in a reduction in proinflammatory cytokines in response to phorbol 12-myristate 13-acetate (PMA)/ionomycin stimulation compared with mock-edited CD4$^+$ T control cells (Figure 8D). Patient-derived FOXP3 cDNA EngTregs also exhibited Treg-associated immunophenotypes, including an increase in CD25, CTLA-4, ICOS, and LAG3, findings distinct from the mock-edited CD4$^+$ controls (Figure 8E). Finally, patient-derived FOXP3 cDNA EngTregs maintained TCR polyclonality similar to the mock-edited cells expanded in parallel (Figure S11).

To demonstrate the requirement for functional correction in IPEX T cells, we next edited T cells from a patient bearing an I363V mutation in the FOXP3 forkhead domain using either the FOXP3 cDNA AAV donor template or our previously reported MND-LNGFR.P2A knockin donor template.[5] Unlike FOXP3 cDNA, MND-driven expression of endogenous FOXP3 I363V failed to reduce tumor necrosis factor α or abolish IL-2 and interferon-γ cytokine production (Figure 8F). These results confirmed that integration and expression of functional FOXP3 cDNA are required for IPEX CD4$^+$ T cells to acquire Treg-like features. These results demonstrate the feasibility of generating functional EngTregs from IPEX patient-derived CD4$^+$ T cells using this candidate therapeutic approach.

DISCUSSION

We have previously reported a gene-editing approach to generate CD4-derived EngTregs as an effective alternative for the generation of therapeutic, immunosuppressive cells. Enforcing endogenous FOXP3 expression in conventional T cells resulted in Treg-like engineered cells.[5] Here, we expand this approach as a potential therapeutic approach for IPEX syndrome. Using AAV HDR donor templates designed to simultaneously disrupt the mutant FOXP3 allele and express a functional FOXP3 cDNA, we demonstrate that seamless integration of the MND promoter and FOXP3 cDNA cassette into coding exon 1 of *FOXP3* leads to high-level FOXP3 expression, co-expression of Treg-associated markers, and a reduction in inflammatory cytokine production. Importantly, we observed equivalent suppressive activity in FOXP3 cDNA EngTreg versus tTreg products both *in vitro* and *in vivo*. Furthermore, adoptive transfer of EngTregs in a surrogate, syngeneic mouse model did not interfere with primary or secondary humoral immune responses, and transfer of autologous human EngTregs in a humanized mouse model did not negatively impact the T cell response to EBV viral infection. Our findings demonstrate efficient generation of EngTregs from CD4$^+$ T cells derived from healthy-donor PB or CB, and, most important, we show efficient EngTreg production using primary T cells from a panel of IPEX subjects. Overall, HDR-mediated, FOXP3 cDNA-driven EngTregs displayed classical Treg immunophenotypes and suppressive function, without compromising the preclinical safety profile, findings that support moving this strategy forward to future clinical application.

FOXP3-cDNA EngTregs exhibit sustained, high-level FOXP3 expression in comparison with the mock-edited controls. However, while expression in FOXP3-cDNA EngTregs is mediated by the introduction of the MND promoter cassette, we observed slightly lower FOXP3 protein levels in comparison with EngTregs designed to express endogenous FOXP3 via MND promoter capture. Several features may account for this modest difference in FOXP3 expression. The *FOXP3* gene contains conserved non-coding sequences (CNSs) that function as enhancers to regulate FOXP3 expression and maintenance. CNS3 is located between the first and second coding exons of *FOXP3* and is absent in the FOXP3 cDNA sequences. In addition, while the FOXP3 cDNA used in this study only encodes the full-length isoform, the endogenous *FOXP3* gene exhibits alternative splicing that leads to the expression of two major splice variants: a full-length FOXP3 isoform and an isoform lacking exon 2 (delta 2 FOXP3).[30] The differences in expression level and function and the balance between these two isoforms are not yet well understood. Despite these differences within the edited *FOXP3* locus and expression level, FOXP3-cDNA EngTregs exhibit significantly higher levels of FOXP3 expression in comparison with tTreg and acquired Treg-like phenotypes and robust suppressive functions. A recent study reported

at the time of secondary immunization (left) and at day 42 (right). (C and D) Graph showing the serum titer of total IgG (C) and high-affinity (NP-4) NP-specific IgG (D) at 0, 9, 28, and 42 days post-immunization with NP-CGG in the presence of the indicated transferred cell populations at the time of secondary challenge. Data shown as mean ± SD; *p* values calculated using *t* test comparing the IgG antibody titer at day 28 versus day 42.

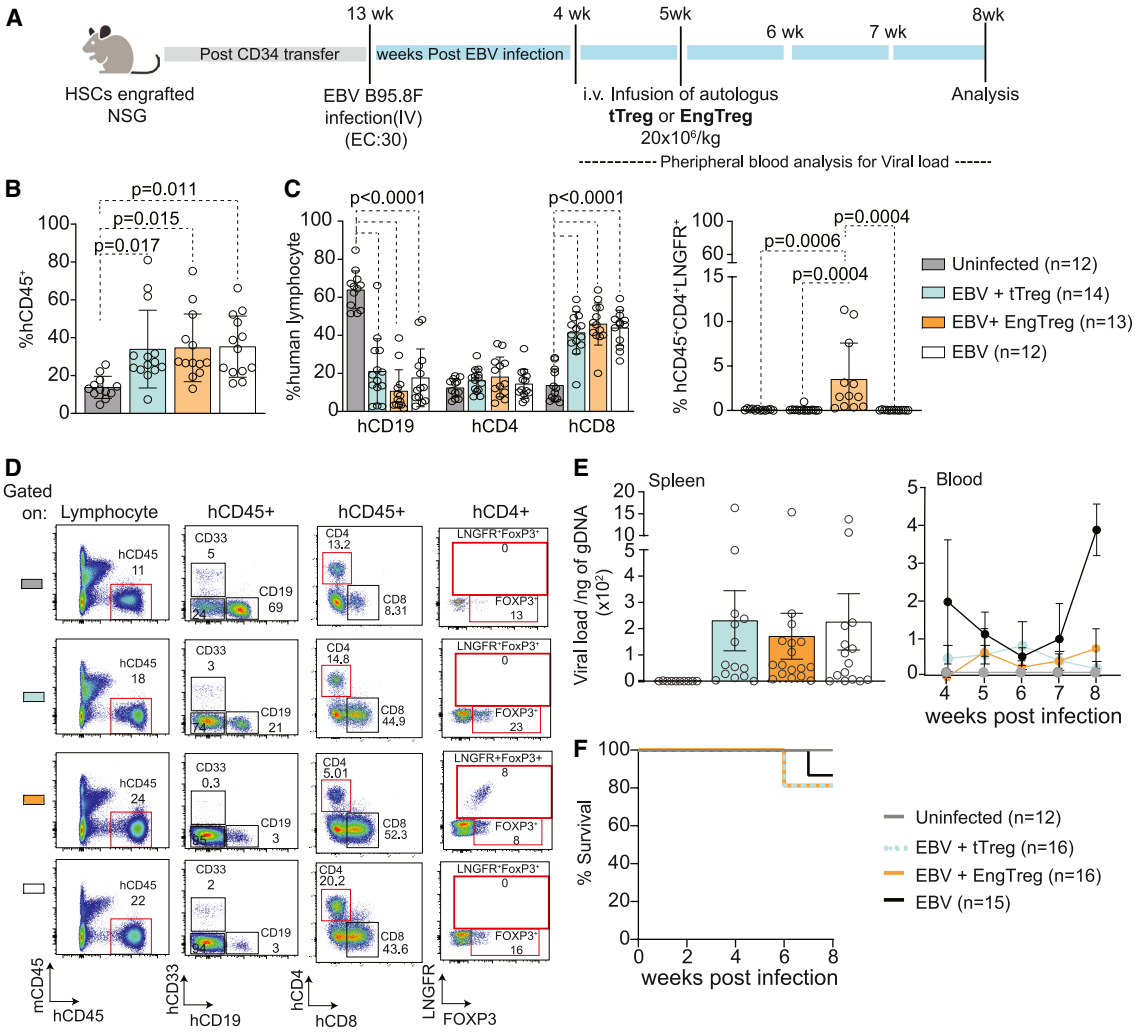

Figure 7. EngTreg do not impact the immune response to EBV infection

(A) Schematic diagram of humanized mouse EBV experiment. Thirteen weeks post-HSPC transfer, humanized NSG mice were infected with EBV virus (strain B95.8F). At 5 weeks post-EBV infection, autologous tTregs or EngTregs were transferred intravenously (20 million cells/kg). Peripheral blood was collected every week starting from 4 weeks post-infection. (B and C) Experimental animals were sacrificed at 8 weeks post-infection, and splenic cells were analyzed to determine the frequency of (B) total hCD45$^+$ cells and (C) human lymphocyte subpopulations: hCD19$^+$, hCD4$^+$, hCD8$^+$, and hCD4$^+$LNGFR$^+$. (D) Representative flow plots from splenic cells showing the gating strategy for human lymphocytes and the presence of EngTreg. hCD33$^+$, hCD19$^+$, hCD4$^+$, and hCD8$^+$ cells were gated from hCD45$^+$ as indicated. hCD4$^+$ were further evaluated for the presence of tTregs by FOXP3$^+$ and EngTregs based on LNGFR$^+$ FOXP3$^+$ staining. (E) Viral load was quantitated in spleen and peripheral blood by ddPCR. Data presented are combined data from four independent experiments, with n = 12 control (no EBV infection); n = 14 EBV-infected humanized mice with infusion of autologous natural Tregs (EBV + tTreg); n = 13 EBV-infected humanized mice, transferred with autologous EngTregs (EBV + EngTreg); and n = 13 EBV-only infected group (EBV). (F) Survival curve of all experimental animals, n = 12 control (no EBV infection); n = 16 EBV + tTreg; n = 16 EBV + EngTreg; and n = 15 EBV-only infected group. Statistical analyses were performed using one-way ANOVA and Sidak multiple comparisons test.

that the co-expression of both FOXP3 isoforms via co-transduction using lentiviral vector (LVV) delivery mediated improved Treg phenotype and function.[31] Of note, the latter approach utilized a less active, EF1α, promoter to drive isoform expression in separate LVVs. Direct comparison between FOXP3-cDNA EngTregs and this dual LVV approach might provide insight regarding the threshold of FOXP3 required to acquire Treg-like features in conventional CD4$^+$ T cells and its correlation to functional outcomes.

In addition to preclinical safety and efficacy, this work demonstrates a scalable, GMP-compatible approach for EngTreg manufacturing. While our work focused primarily on generating EngTregs from CD4$^+$ T cells isolated from leukapheresis products, EngTregs were also efficiently generated using CB CD4$^+$ T cells, and these products exhibited suppression of allogeneic effector T cells in a xeno-GvHD model. Most important, FOXP3-cDNA EngTregs generated from IPEX patient-derived CD4$^+$ T cells isolated from whole blood

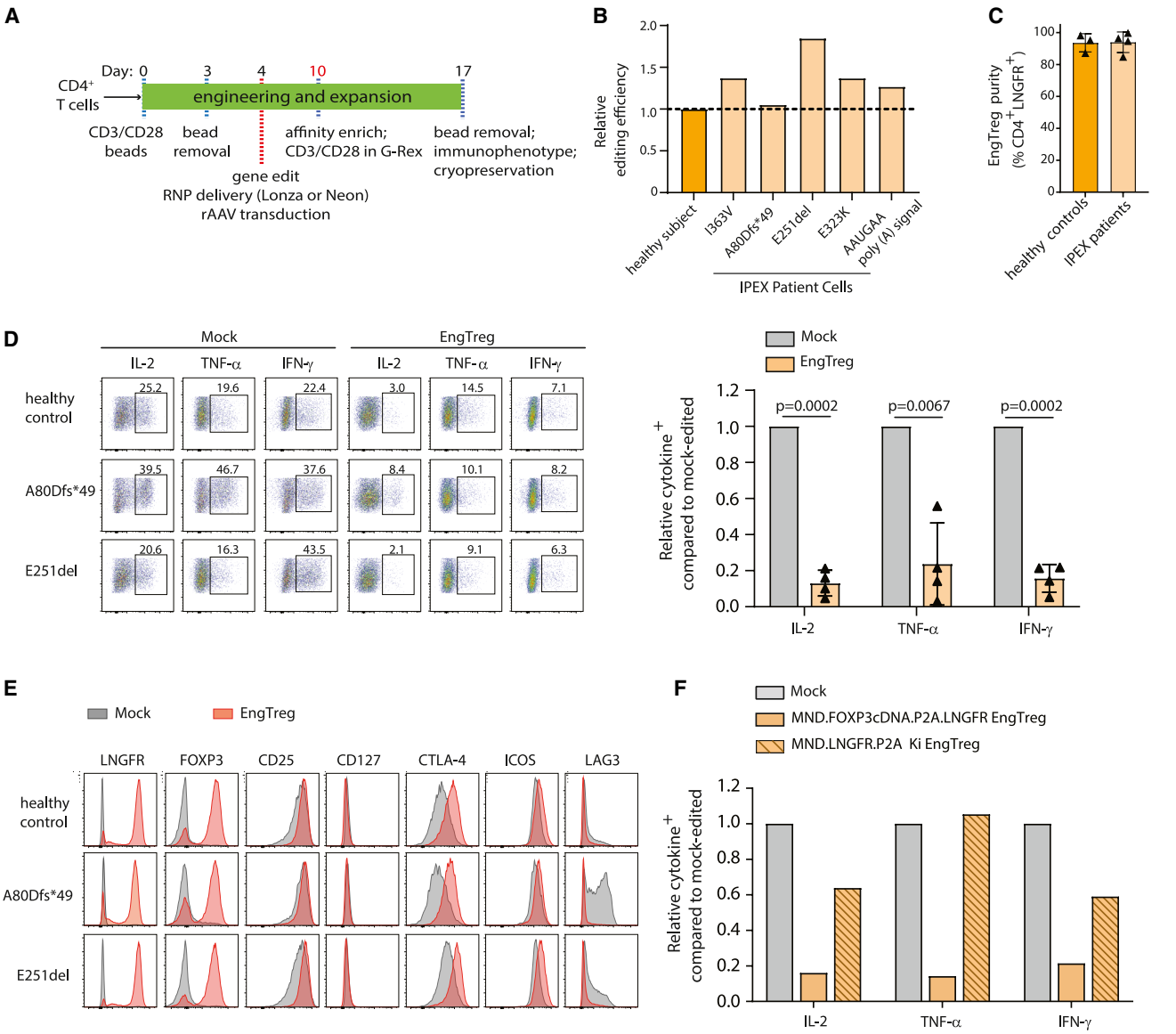

Figure 8. Generation of EngTregs from CD4⁺ T cells of IPEX patients

(A) Schematic of EngTreg production from IPEX patient-derived CD4⁺ T cells. CD4⁺ T cells from healthy donors were edited in parallel as experimental control. Modifications from the preclinical process described in Figure 2A due to limited cell numbers available are marked in red. Briefly, edited cells were expanded for an additional 3 days prior to LNGFR affinity enrichment. CD4⁺ T cells from a healthy subject were processed with the modified protocol in parallel as a control. (B) Graph shows mean ± SD of editing efficiency of IPEX CD4⁺ T cells measured by flow cytometry as percent LNGFR⁺ in live single CD4⁺ cells 2 days after editing. (C) Purity measured as percent LNGFR⁺ in live CD4⁺ T cells of IPEX patient-derived EngTreg upon completion of the production process at day 17, described in the schematic. Graph shows mean ± SD from four independent patient cell products. (D) Representative flow plots (left) and graph (right; mean ± SD, $n = 4$) of intracellular cytokine staining in mock-edited or EngTreg cells after a 5-h stimulation with PMA/ionomycin in the presence of GolgiStop. Relative cytokine positivity compared to autologous mock-edited cells is graphed. p values calculated by t test. (E) Representative histograms of LNGFR and Treg-associated markers in EngTreg (orange) and mock-edited cells (gray) generated from two IPEX subjects or a healthy control. Flow cytometry analysis for each marker was gated in live singlet CD4⁺ T cells. (F) Inflammatory cytokine positivity of IPEX CD4⁺ T cells that were mock edited or gene edited to express MND-driven functional FOXP3cDNA (MND.FOXP3cDNA.P2A.LNGFR EngTreg) or endogenous I363V FOXP3 mutation (MND.LNGFR.P2A.Ki EngTreg). Intracellular cytokine staining was analyzed after PMA/ionomycin stimulation in the presence of GolgiStop. Relative cytokine positivity compared to autologous mock-edited cells was graphed.

acquired Treg marker expression and reduced inflammatory cytokine production. The only current curative treatment for IPEX is allogeneic HSCT.[14,15,32,33] However, this approach remains limited due to donor availability, complications of ongoing clinical autoimmune disease, as well as peri- and post-transplant morbidity.[15] CD4-derived EngTregs might provide a safe and effective treatment

option prior to HSCT, or possibly, in lieu of HSCT. Notably, $CD4^+$ T cells in IPEX patients are predicted to be enriched for self-reactive TCRs[34] that mediate loss of immune tolerance; thus, capturing this TCR repertoire is likely to promote targeting to tissue-specific inflammatory sites. We demonstrate that HDR editing of $CD4^+$ T cells generates EngTregs with a broad TCR repertoire based upon β chain spectratype analysis of products from three IPEX patients with differing FOXP3 mutations, as well as spectratype analysis and deep sequencing of the TCR β chain of EngTreg products from two healthy donors. Furthermore, we show that EngTregs remained viable and capable of proliferating in response to TCR engagement in the presence of immunosuppressant drugs utilized to control IPEX disease activity, suggesting that patients might not be required to discontinue immunosuppressant therapy prior to or following EngTreg infusion. Finally, we performed a direct analysis of the potential safety risks of surrogate murine EngTregs and human FOXP3-cDNA EngTregs, respectively, in the setting of a primary or secondary TD immune response and during ongoing viral infection. Our studies identified no evidence for an altered immune response in these contexts. This combined dataset supports the concept that adoptive transfer of patient-derived, FOXP3-cDNA EngTregs may have the potential for clinical benefit in IPEX.

To date, several approaches have been developed to generate immunosuppressive cellular products from $CD4^+$ T cells, including small-molecule-mediated generation of induced Treg (NCT01634217),[35] LVV-mediated gene transfer (NCT05241444),[36] and HDR FOXP3 gene editing. Despite the difference in methodologies, a common and key concept is the expression of FOXP3 in conventional $CD4^+$ T cells. Generation of immunosuppressive cell products using bulk $CD4^+$ T cells holds manufacturing advantages in comparison with the challenges of isolation and expansion of tTregs. For example, the abundance of $CD4^+$ T cells in source materials, including leukapheresis products, whole PB, or CB makes the cell isolation and expansion to target dose less cumbersome. Similarly, the lack of a single unique surface marker to identify tTregs makes it technically challenging and costly to isolate thymic-derived Tregs at high purity and lack contaminating effector T cells. In addition, decreased cell quantities or dysfunctional tTregs have been associated with autoimmune diseases and may not be suitable for the manufacturing and expansion of tTregs; this challenge is particularly relevant to IPEX, where tTregs are absent or markedly reduced and/or dysfunctional.

A lentiviral approach for FOXP3 gene transfer into $CD4^+$ T cells of IPEX patients showed conversion to Treg phenotype and function.[36] An ongoing phase 1 clinical trial (NCT05241444) at Stanford University using LVVs to express FOXP3 cDNA in autologous IPEX patient $CD4^+$ T cells represents a significant milestone for the IPEX immunotherapy. In this approach, the *FOXP3* locus carrying the mutation remains unaltered and is predicted (depending on the genetic lesion) to lead to expression of the endogenous, mutant FOXP3 protein in T cells that failed to undergo efficient Treg differentiation and/or in the setting of activation-mediated FOXP3 transcription. The resulting FOXP3 mutant protein might dimerize with the ectopically expressed functional FOXP3 transgene and thus potentially impede optimal FOXP3 function as a transcription factor. The *FOXP3* gene editing approach described here disrupts the expression of endogenous, mutated FOXP3 and replaces it with a functional FOXP3 cDNA. Furthermore, in contrast to LVV delivery, HDR editing concurrently controls for single-copy integration of the FOXP3 cassette. Thus, the FOXP3cDNA-EngTreg approach removes these potential concerns and may be more potent than the LVV approach. In addition, site-specific gene editing and integration not only provides a uniform expression of FOXP3 transgene but also could be a safer and potentially more persistent approach than LVV delivery. As previously shown, random viral integration is subject to transgene silencing[5] and adds a potential risk of activation of proto-oncogenes or inhibition of tumor suppressors at sites of integration. FOXP3 mutations identified in IPEX patients are distributed throughout the *FOXP3* gene.[20] Correction of patient-specific FOXP3 mutations is feasible with the recent progress in base-, prime- and/or alternative gene-editing technologies. However, the FOXP3cDNA EngTreg approach is designed to provide a universal treatment for IPEX patients regardless of the specific mutations in the *FOXP3* locus. While the use of AAV6 to deliver the HDR donor template in our production strategy may increase production costs, alternative non-viral approaches could be explored in the future.[37–40]

With the advancement of chimeric antigen receptor (CAR) and TCR engineering, antigen-specific cell therapies provide specificity and reduce potential off-target effects. For autoimmune disorders with identified antigens such as T1D or RA, incorporation of antigen-specific CAR or TCR into EngTregs via LV or gene editing[6,9] may provide an optimal path to enhance both efficacy and safety by increasing the target specificity and enabling the cell dose de-escalation. Importantly, in IPEX and potentially other settings (HSCT, solid organ transplantation, inflammatory diseases without defined target antigens) polyclonal EngTreg may be best suited to mitigate systematic inflammatory responses. Importantly, our data indicate that EngTregs retain a diverse TCR clonality comparable to parental bulk $CD4^+$ T cells and would be predicted to respond to multiple antigens. In addition, EngTregs generated from $CD4^+$ T cells derived from IPEX patients are predicted to be enriched for self-antigen-specific TCRs[34] and thus likely to suppress a broad range of autoreactive effector T cells and rebuild immune tolerance. Long-term engraftment of EngTreg will likely be required for sustained efficacy in IPEX patients. The absence of an endogenous tTreg compartment and higher IL-2 levels in IPEX patients may be sufficient to achieve sustained engraftment and long-term benefit. Consistent with engraftment in the absence of conditioning, our syngeneic mouse studies demonstrate the presence of EngTregs in immunocompetent hosts for up to 42 days post-adoptive transfer. Repeated EngTreg dosing, as performed in our mouse humoral response studies, offers a potential option for improved EngTreg response. Alternatively, cell-intrinsic IL-2 support provided by a prevously described engineered chemically inducible signaling complex[7] may also facilitate clinical benefit. Future work will help further refine an optimal EngTreg platform and trial design for clinical efficacy in IPEX patients.

MATERIALS AND METHODS

Gene editing and AAV vector design

Several CRISPR gRNAs targeting the first coding exon of *FOXP3* gene were selected from the CRISPR-Cas9 target online predictor CCTop (https://crispr.cos.uni-heidelberg.de/) for initial on-target efficiency assessment. The lead T9 gRNA targeting 5′-TCCAGCTGGGCGAGGCTCCT-3′ with the protospacer-adjacent motif sequence GGG corresponds to nucleotides 49,258,427–49,258,449 of the chrX in the GRCh38 (hg38) human genome assembly. The chemically modified 100-mer sgRNA was synthesized with 2′O-methyl analogs and 3′ phosphorothioate inter-nucleotide linkages in the first and last three nucleotides (Synthego or Biospring) (Table S1). The sgRNA was reconstituted in sterile RNase-free Tris-EDTA buffer, pH 8.0 (Fisher) and stored at −80°C. For the assembly of the Cas9 and sgRNA RNP complex, Alt-R Cas9 (IDT) or SpyFi Cas9 (Aldevron) protein was incubated with sgRNA at room temperature for 20 min with a 1:2.5 molar ratio. RNP complex containing 80 pmol Cas9 and 200 pmol sgRNA were delivered to each 1×10^6 activated $CD4^+$ T cell via nucleofection or electroporation.

The AAV vectors containing a gene expression cassette flanked by 5′ and 3′ homology sequences to the gRNA target site on *FOXP3* were generated following the methods described previously.[5] Briefly, the Cas9/T9 gRNA-mediated cleavage occurs between nucleotides 49,258,443 and 49,258,444 of the chrX in the hg38 human genome assembly. DNA sequences mapped to 49,258,447–49,259,046 and 49,257,843–49,258,442 were cloned into the AAV vectors between the two inverted terminal repeats (ITRs) as the 5′ and 3′ HAs. The gene expression cassette containing an MND promoter coding sequences of full-length human FOXP3 cDNA in frame with a P2A ribosomal skip peptide, followed by the extracellular and transmembrane coding sequences of human LNGFR and SV40 poly(A), were PCR amplified or gene synthesized (IDT). The expression cassette was subsequently cloned into the restriction endonuclease linearized AAV vector between the 5′ and 3′ HAs by In-Fusion Cloning (Takara). The resulting plasmid DNA containing the expression cassette of MND-FOXP3cDNA.P2A.LNGFR-poly(A) flanked by 0.6-kb *FOXP3* HAs was sequence verified before AAV generation.

Viral vector production

Recombinant AAVs were generated in HEK293T cells as described previously[41] and then purified with AVB Sepharose (GE), followed by iodixanol ultracentrifugation. AAV serotype 6 was used for human T cell transduction, while serotype 5 was used for mouse T cell transduction. Some purified AAVs were further formulated in 1× PBS containing 200 mM NaCl and 0.001% poloxamer-188. Viral titers were determined by qPCR or ddPCR using ITR-specific primers.[41]

Isolation and activation of primary human $CD4^+$ T cells for gene editing

Human PBMCs isolated from leukapheresis collection of healthy donors were purchased from the Co-operative Center for Excellence in Hematology Cell Processing Core Facility at Fred Hutchinson Cancer Research Center (Seattle, WA). IPEX patient mononuclear cells from PB draw (PBMCs) or CB were obtained from Seattle Children's Hospital clinicians. Obtained informed consent was reviewed and approved by the institutional review boards of the Fred Hutchinson Cancer Research Center (FH985.03) or the Seattle Children's Research Institute (SCRI; 11738), respectively. Additionally, fresh healthy CB was purchased from Bloodworks or GenCure and processed for mononuclear cell isolation. Isolated mononuclear cells were viably frozen and stored in the liquid nitrogen vapor phase freezers.

$CD4^+$ T cells were enriched from thawed mononuclear cells using a negative selection method (EasySep Human $CD4^+$ T cell Enrichment Kit, catalog no. 19052, STEMCELL Technologies), then either directly cultured for gene editing or frozen down for later use. Prior to gene editing, $CD4^+$ T cells were cultured at 0.5 million/mL in T cell culture media for 72 h with Dynabeads Human T-Expander CD3/CD28 (catalog no. 11141D, Thermo Fisher Scientific) at a 3:1 ratio of beads to cells. The T cell culture media was composed of RPMI 1640 (Hyclone), 20% fetal bovine serum (catalog no. FB-11, Omega Scientific), 10 mM HEPES (Gibco), 2 mM GlutaMax (Gibco), 55 μM β-mercaptoethanol (Gibco), and 50 ng/mL human IL-2 (PeproTech). After 72 h of incubation, beads were removed by magnetic separation, and cell cultures were continued for an additional 18–24 h at 0.5 million/mL before editing.

HDR-mediated gene editing by Cas9 RNP delivery and AAV transduction

Neon transfection system (Invitrogen), 4D-Nucleofector (Lonza), and Maxcyte GT (Maxcyte) were used to deliver Cas9/sgRNA RNP into activated human $CD4^+$ T cells. Prior to Cas9 RNP delivery, cells were washed twice with 1× PBS and resuspended in buffer T, supplemented P3 buffer, and Maxcyte electroporation buffer, respectively, at the manufacturers' recommended concentration. RNP was then added into cell resuspension and immediately underwent electroporation or nucleofection using the following settings: Neon (1,420 V, 10 ms, 3 pulses), Lonza 4D-Nucleofector (DN-102 or EO-115), and Maxcyte GT (expanded T cell 1-OC). Treated cells were transferred to culture vessels containing T cell media followed by AAV6 transduction with 20% v/v and incubated at 37°C with 5% CO_2. As a control, cells were delivered with Cas9 alone in the absence of sgRNA and then incubated with AAV donor template as mock-edited cells. In some experiments, AAV transduction was initially performed in the serum-free media for 2 h before adding fetal bovine serum (FBS) to cell culture to a final concentration between 10% and 12.5%. Approximately 24 h later electroporation and AAV transduction, cell culture was transferred to a larger vessel, and an equal volume of fresh complete media was added to dilute AAV concentration. Editing efficiency was determined by measuring the cell surface expression of LNGFRt using flow cytometry approximately 48 h after editing. The percentage of $LNGFR^+$ in live singlet $CD4^+$ T cells was analyzed for gene editing efficiency. For murine EngTreg production, activated mouse $CD4^+$ T cells were delivered by RNP containing a mouse Foxp3 sgRNA (target sequence: 5′-CCAGCUUGGCAAGACUCCUG-3′) using the

Neon transfection system, followed by incubation with AAV5-containing donor template with homology sequence to mouse *Foxp3*, as previously described.[6]

Affinity enrichment, cell expansion, and cryopreservation

Edited cells expressing intracellularly LNGFRt as a surface marker were enriched 3 days after editing using the human CD271 microbead kit (Miltenyi Biotec, catalog no. 130-099-023). For each 1×10^7, cells were resuspended in 80 μL per pre-chilled magnetic-activated cell sorting (MACS) separation buffer containing 1× PBS, 0.5% FBS, and 2 mM EDTA, followed by incubation with 25 μL FcR blocking reagent and 25 μL CD271 microbeads at 4°C for 15 min. After incubation, 2 mL MACS separation buffer was added per 1×10^7 cells before centrifugation at 300 × *g* for 5 min. Single-cell suspension in MACS separation buffer was then loaded onto the MACS LS columns (Miltenyi) placed in the magnetic field of an MACS separator. After washing the columns four times with a 3-mL MACS separation buffer, columns were removed from the separator, and the bound cells were eluted from the columns with a 5-mL MACS separation buffer using the provided plunger. Approximately 1.5–2 million enriched cells were plated in each G-Rex10 flask or G-Rex 6-well plate with Dynabeads Human T-Expander CD3/CD28 beads at a 3:1 bead-to-cell ratio. A final volume of 30 mL Treg expansion media containing 100 ng/mL human IL-2 and 100 nM rapamycin (Sigma-Aldrich) was added to each G-Rex well for expansion. On the 3rd and 5th days of G-Rex culture, 15 mL culture media in the G-Rex vessels was carefully removed from the top, and the remaining culture volume was resuspended by gentle pipetting to de-cluster the bead-bound cells before adding 15 mL fresh expansion media containing IL-2. No additional rapamycin was added to culture during expansion. After a 7-day culture in G-Rex, cells were collected from G-Rex, and CD3/CD28 beads were removed by magnetic separation, followed by viable cryopreservation using Cryostor CS10 media (STEMCELL Technologies).

Isolation and expansion of tTregs

Human tTregs purified from autologous PBMCs using the EasySep Human $CD4^+CD127^{lo}CD25^+$ Regulatory T cell Isolation Kit (STEMCELL Technologies) were expanded in Treg expansion media with either Dynabeads Human T-Activator or T-Expander CD3/CD28 (Thermo Fisher Scientific) beads following the manufacturer's recommended ratio. Cell culture was expanded and maintained at 0.5–1 million cells per milliliter of media for the first 7 days. On day 7, initial beads were removed from culture by magnetic separation and fresh beads were added before plating in G-Rex 6-well plates at 1.5–2 million cells per well in 30 mL expansion media and 100 nM rapamycin. To match the expansion protocol of EngTreg, half volume of the culture media was removed from tTreg expansion and replaced with fresh expansion media every 2–3 days, and cells were resuspended at each media refreshment. At the end of the expansion procedure, magnetic beads were removed from cell culture, and expanded tTregs were cryopreserved in Cryostor CS10 freezing media. In each cell expansion, the $CD4^+CD25^-$ fraction from Treg isolation was expanded in parallel as conventional T cells control.

Molecular detection of gene editing and HDR efficiency

Genomic DNA extracted from expanded engineered $CD4^+$ T cells using the DNeasy Blood & Tissue kit (QIAGEN) was subjected to conventional PCR and ddPCR analysis to measure NHEJ or HDR. For on-target and off-target NHEJ detection, cells treated with Cas9/gRNA RNP in the absence of AAV were harvested 3–7 days after editing. For HDR analysis, cells were collected after G-Rex expansion or from cryopreserved EngTreg. PCRs were carried out using PrimeSTAR GXL (Clontech) or AccuPrime Pfx (Thermo Fisher Scientific) DNA polymerase and oligonucleotide primers, as seen in Table S2. PCR amplicons were resolved using electrophoresis in agarose gels, extracted using Zymoclean Gel DNA Recovery Kit (Zymogen) and then sequenced using Sanger sequencing (Genewiz). Sequencing reads were aligned with reference sequences or analyzed for percent indel using Inference of CRISPR Edits (ICE) software (Synthego). In experiments where colony sequencing was performed, purified PCR products were first cloned into pJET1.2/blunt vector using the CloneJET PCR Cloning Kit (Thermo Fisher Scientific), and the resulting colonies were individually sequenced.

ddPCR assays were performed using the QX200 Droplet Digital PCR system (Bio-Rad) following the manufacturer's instruction manual. The oligonucleotide primers and probes are listed in Table S2. The primer pairs used to amplify the HDR-edited *FOXP3* locus target the 3′ region of LNGFR and immediately downstream of the 3′ HA, respectively, while the reference control primer pairs amplify sequences 6,728 bp downstream of the Cas9 cleavage site (alternatively, 6,127 bp downstream of integration at *FOXP3* [from 3′ end of 3′ HA]). Reaction mixtures containing ddPCR Supermix (Bio-Rad), genomic DNA (50 ng), primers, and probes for both HDR and reference control detection were subjected to droplet generation followed by PCR amplification and droplet quantification. Data were analyzed using QuantaSoft (Bio-Rad) with a positive threshold set at 2,000 amplitudes. Percent HDR was calculated as the ratio of the HDR concentration to the reference control concentration.

Flow cytometry

Aliquots of cells post-thaw or grown in culture were used for surface immunostaining with fluorescent antibodies (Table S3) and a viability dye (Near-IR LIVE/DEAD Fixable Dead Cell Stain Kit or Alexa Fluor 350 carboxylic acid NHS ester, Invitrogen). In some cases when cells were fixed and permeabilized to detect intracellular proteins, the True-Nuclear Transcription Factor Buffer Set (BioLegend) was used for FOXP3, CTLA-4, and Helios detection, and BD Cytofix/Cytoperm Fixation/Permeabilization Solution Kit (BD Biosciences) was used for intracellular cytokine staining. To detect intracellular cytokines, cells were cultured in media containing 20 ng/mL PMA (MilliporeSigma), 1 μg/mL ionomycin (MilliporeSigma), and 1 μg/mL Golgi-Stop (BD Biosciences) for 5 h at 37°C before staining. To detect TGF-β expression, cells were activated with anti-CD3/CD28 Dynabeads overnight before staining with viability dyes and surface

expression of GARP and LAP. All procedures including surface staining, fixation, permeabilization, and intracellular staining were performed according to the manufacturers' protocols with the exception of 90-min fixation when using the True-Nuclear Transcription Factor Buffer Set. A BD LSR II flow cytometer and FACSDIVA software (BD Biosciences) were used for fluorescence detection and data acquisition. Flow cytometry data were analyzed using FlowJo software version 10.5 and later (Becton Dickinson). Marker expressions were analyzed in live singlet $CD4^+$ T cells.

Immunosuppression assays

Cryopreserved autologous responders ($CD4^+$ or $CD4^+CD25^-$ T cells) and suppressors were thawed and rested for 90 min at 37°C prior to assay setup in T cell culture media in the absence of IL-2. Responders were labeled with the Cell Trace Violet (CTV) Proliferation Kit (Thermo Fisher Scientific) and plated in 96-well plates at 2.5×10^4 cells per well. Suppressors were stained with Cell Proliferation Dye eFluor 670 (eBioscience) and plated at various suppressor-to-responder ratios between 8:1 and 1:32. Human T-Activator CD3/CD28 beads were added at a bead-to-cell ratio of 1:10 to stimulate theproliferation of responders. Wells containing CTV-labeled responders only with or without beads were included as positive and negative controls, respectively. Each condition was set up in duplicate and incubated for 72–96 h before pooling for flow cytometry. The percentage proliferation of each sample was compared to the percent proliferation of bead-stimulated responder-only control. Percent suppression was calculated with the described equation: percent suppression = ([% proliferation of responders without suppressors] − [% proliferation of responders with suppressors]/[% proliferation responders without suppressors] × 100).

Immunosuppressive drug studies

Mock-edited $CD4^+$ T cells and EngTreg were thawed and rested for 72 h in T cell media supplemented with 5 ng/μL human IL-2 (PeproTech). All cells were then stimulated for 24 h with Dynabeads Human T-Expander CD3/CD28 (Thermo Fisher Scientific) at a 2:1 bead-to-cell ratio. Cells were then washed and plated into 96-well plates holding the drug dosage conditions in T cell media, 100,000 cells per condition in a 100-μL final volume. After 72 h, cell concentration and viability were measured using the MUSE Cell Counter (Luminex) according to the manufacturer's instructions. Cells were then re-plated in fresh drug-containing media at equal cell concentrations. After an additional 72 h, cell numbers and viability were taken for a final time point. All drugs were obtained from MilliporeSigma and were reconstituted according to the manufacturer's instructions. Final drug dilutions were made in T cell media, and the dose ranges for all drugs were 1, 10, 100, and 1,000 nM. For analysis of growth and viability, treated groups were compared to relevant untreated mock-edited $CD4^+$ T or EngTreg groups cultured in parallel.

Mouse studies overview

NSG (NOD.Cg-Prkdc^{scid} Il2rg^{tm1Wjl}/SzJ) and CD45.1 and CD45.2 C57Bl/6 (B6) mice were originally obtained from The Jackson Laboratory (Jax) and housed in a specific pathogen-free Association for Assessment and Accreditation of Laboratory Animal Care-accredited facility at SCRI. All experimental mice were either bred in-house or purchased directly from Jax. Animal studies and procedures were approved by the Institutional Animal Care and Use Committee of SCRI and performed in accordance with the NIH *Guide for the Care and Use of Laboratory Animals*.

Xenograft-induced GvHD

Male NSG mice at 8–12 weeks of age were treated with 200 cGy total body irradiation approximately 2 h before Treg infusion. Cryopreserved EngTreg, tTreg, and mock-edited $CD4^+$ T cells were thawed, washed, and resuspended in PBS; 8×10^6 cells resuspended in 200 μL PBS were I.V. injected into each mouse through the tail vein. Three days later, mice were I.V. injected with 100 μL PBS containing 4×10^6 $CD4^+$ Teff freshly isolated from thawed autologous PBMCs (EasySep Human $CD4^+$ T cell Enrichment Kit, STEMCELL Technologies). Baytril (enrofloxacin, 0.2 mg/mL; Bayer Healthcare) was supplemented in drinking water for irradiated mice for 14 days following irradiation. Animals were monitored for health and weight loss three times weekly and assessed for symptoms of GvHD once weekly for the study. GvHD onset and progression was assessed according to the previously established scoring system[42] to measure weight change, posture, activity, fur texture, and skin integrity (Table S4). Mice that lost over 20% of their body weight measured at the time of irradiation were euthanized for humane purposes or otherwise sacrificed at the end of the experiment. Upon sacrifice, cells isolated from PB, spleen, liver, and lung were immunostained for flow cytometry analysis.

Safety study in syngeneic immunocompetent murine model

The 8- to 12-week-old B6 male mice were immunized through intraperitoneal injection with 200 μL emulsion containing 100 μg NP-CGG (catalog no. N-5055 E-5, Biosearch Technologies) and 100 μL of alum (catalog no. 77161, Thermo Scientific). For recall response, mice were intraperitoneally injected with 100 μg NP-CGG in a total volume of 200 μL at day 28 post-primary immunization. To test total serum IgG and NP-specific IgG antibody titers, 96-well Nunc-Immuno MaxiSorp plates (Thermo Scientific) were coated with anti-IgG or NP-BSA and incubated overnight at 4°C. Plates were then blocked for 1 h with 2% BSA in PBS before the addition of diluted serum for a 2-h incubation at room temperature. Antibodies were detected using goat anti-mouse IgG horseradish peroxidase (Southern Biotech). The peroxidase reaction was developed via OptEIA TMB substrate (BD Biosciences) and stopped with sulfuric acid; the plate was read at 450 nm using a SpectraMax 190 microplate (Molecular Devices).

EBV infection model

Thawed human $CD34^+$ cells collected from granulocyte-colony-stimulating factor-mobilized apheresis were injected via retro-orbital injection to 8- to 10-week-old female NSG mice at 1 million cells in 200 μL PBS per mouse. After 13 weeks, an aliquot of peripheral blood was collected to confirm engraftment before EBV infection as previously described.[29] EBV was generated as previously

described[43] and was injected into the humanized mice via the retro-orbital route. Four weeks post-EBV infection PB was sampled as baseline, and 20 × 10^6 cells/kg tTregs or EngTregs derived from autologous PBMCs were infused to each mouse via tail vein at the following week. Mice were then monitored weekly for body weight and general health condition. Blood draws were performed weekly to monitor viral load by ddPCR. Mice were sacrificed 3 weeks after T cell transfer, and PB and bone marrow were analyzed for the presence of human B and T lymphocytes and viral load by flow cytometry and ddPCR, respectively.

Statistical analysis

All data were graphed as mean ± SD (standard deviation) or mean ± SEM (standard error of the mean). All statistical analyses were performed using Prism (version 8, GraphPad Software), and the methods used are indicated in the figure legends accordingly. All *in vitro* assays were performed with three or more biological replicates. All the *in vivo* studies were performed with two or more biological replicates, with a minimum of 3 mice in each group in each study.

DATA AND CODE AVAILABILITY

Data supporting the findings of the present study are available upon request from the corresponding author.

ACKNOWLEDGMENTS

We thank Jennifer Haddock for assistance with editing the manuscript and Laura Smith for project management and coordination. Additionally, we thank Claire Stoffers, Stefan Lachkar, and Anna Zielinska-Kwiatkowska for technical assistance with mouse studies. We also thank the members of the Rawlings laboratory for helpful discussions and support. This work was supported in part by sponsored research agreements with Casebia Therapeutics and Gentibio. This work was also supported by the Seattle Children's Research Institute Program for Cell and Gene Therapy, the Children's Guild Association Endowed Chair in Pediatric Immunology (to D.J.R.), and the Hansen Investigator in Pediatric Innovation Endowment (to D.J.R.).

AUTHOR CONTRIBUTIONS

Y.H. and D.J.R. conceptualized and designed the study. Y.H. generated and tested AAV constructs, developed the gene editing and expansion process, and produced and characterized T cell products. N.P.D. led and performed the *in vivo* GvHD studies. S.S. led and performed the EBV studies. A.K.S. led and performed the humoral immune response studies. C.L. performed the *in vitro* suppression assays and assisted with EBV viral production. D.G. assisted with humoral immune response and GvHD studies. S.S. and H.J. performed the ddPCR assays. S.S. assisted with the immunosuppressive drug studies. H.J. performed the TCR sequence analysis. S.P. assisted with T cell product characterization. I.F.K. generated AAV for the study. M.L.C. led and performed the immunosuppressive drug studies. S.J.Y. performed immunostaining for LAP/GARP. C.E.K.I., G.I.U., and G.J.C. performed GUIDE sequencing and amplicon sequencing. T.R.T. and E.J.A. provided IPEX patient samples. Y.H., P.J.C., K.S., and D.J.R. wrote the manuscript, with assistance from additional co-authors. D.J.R. obtained the funding and was responsible for the project.

DECLARATION OF INTERESTS

D.J.R. is scientific co-founder, scientific advisor, and scientific advisory board member of GentiBio. Y.H., I.F.K., K.S., T.R.T., and D.J.R. are inventors on patents describing methods detailed in this paper.

SUPPLEMENTAL INFORMATION

Supplemental information can be found online at https://doi.org/10.1016/j.ymthe.2026.03.017.

REFERENCES

1. Bayati, F., Mohammadi, M., Valadi, M., Jamshidi, S., Foma, A.M., and Sharif-Paghaleh, E. (2020). The Therapeutic Potential of Regulatory T Cells: Challenges and Opportunities. Front. Immunol. *11*, 585819. https://doi.org/10.3389/fimmu.2020.585819.

2. McCallion, O., Bilici, M., Hester, J., and Issa, F. (2023). Regulatory T-cell therapy approaches. Clin. Exp. Immunol. *211*, 96–107. https://doi.org/10.1093/cei/uxac078.

3. Amini, L., Kaeda, J., Fritsche, E., Roemhild, A., Kaiser, D., and Reinke, P. (2022). Clinical adoptive regulatory T Cell therapy: State of the art, challenges, and prospective. Front. Cell Dev. Biol. *10*, 1081644. https://doi.org/10.3389/fcell.2022.1081644.

4. Bluestone, J.A., McKenzie, B.S., Beilke, J., and Ramsdell, F. (2023). Opportunities for Treg cell therapy for the treatment of human disease. Front. Immunol. *14*, 1166135. https://doi.org/10.3389/fimmu.2023.1166135.

5. Honaker, Y., Hubbard, N., Xiang, Y., Fisher, L., Hagin, D., Sommer, K., Song, Y., Yang, S.J., Lopez, C., Tappen, T., et al. (2020). Gene editing to induce FOXP3 expression in human CD4(+) T cells leads to a stable regulatory phenotype and function. Sci. Transl. Med. *12*, eaay6422. https://doi.org/10.1126/scitranslmed.aay6422.

6. Yang, S.J., Singh, A.K., Drow, T., Tappen, T., Honaker, Y., Barahmand-Pour-Whitman, F., Linsley, P.S., Cerosaletti, K., Mauk, K., Xiang, Y., et al. (2022). Pancreatic islet-specific engineered T(regs) exhibit robust antigen-specific and bystander immune suppression in type 1 diabetes models. Sci. Transl. Med. *14*, eabn1716. https://doi.org/10.1126/scitranslmed.abn1716.

7. Cook, P.J., Yang, S.J., Uenishi, G.I., Grimm, A., West, S.E., Wang, L.J., Jacobs, C., Repele, A., Drow, T., Boukhris, A., et al. (2023). A chemically inducible IL-2 receptor signaling complex allows for effective in vitro and in vivo selection of engineered CD4+ T cells. Mol. Ther. *31*, 2472–2488. https://doi.org/10.1016/j.ymthe.2023.04.021.

8. Hunt, M.S., Yang, S.J., Mortensen, E., Boukhris, A., Buckner, J., Cook, P.J., and Rawlings, D.J. (2023). Dual-locus, dual-HDR editing permits efficient generation of antigen-specific regulatory T cells with robust suppressive activity. Mol. Ther. *31*, 2872–2886. https://doi.org/10.1016/j.ymthe.2023.07.016.

9. Uenishi, G.I., Repic, M., Yam, J.Y., Landuyt, A., Saikumar-Lakshmi, P., Guo, T., Zarin, P., Sassone-Corsi, M., Chicoine, A., Kellogg, H., et al. (2024). GNTI-122: an autologous antigen-specific engineered Treg cell therapy for type 1 diabetes. JCI Insight *9*, e171844. https://doi.org/10.1172/jci.insight.171844.

10. Powell, B.R., Buist, N.R., and Stenzel, P. (1982). An X-linked syndrome of diarrhea, polyendocrinopathy, and fatal infection in infancy. J. Pediatr. *100*, 731–737. https://doi.org/10.1016/s0022-3476(82)80573-8.

11. Chatila, T.A., Blaeser, F., Ho, N., Lederman, H.M., Voulgaropoulos, C., Helms, C., and Bowcock, A.M. (2000). JM2, encoding a fork head-related protein, is mutated in X-linked autoimmunity-allergic disregulation syndrome. J. Clin. Invest. *106*, R75–R81. https://doi.org/10.1172/JCI11679.

12. Bennett, C.L., Christie, J., Ramsdell, F., Brunkow, M.E., Ferguson, P.J., Whitesell, L., Kelly, T.E., Saulsbury, F.T., Chance, P.F., and Ochs, H.D. (2001). The immune dysregulation, polyendocrinopathy, enteropathy, X-linked syndrome (IPEX) is caused by mutations of FOXP3. Nat. Genet. *27*, 20–21. https://doi.org/10.1038/83713.

13. Barzaghi, F., Passerini, L., and Bacchetta, R. (2012). Immune dysregulation, polyendocrinopathy, enteropathy, x-linked syndrome: a paradigm of immunodeficiency with autoimmunity. Front. Immunol. *3*, 211. https://doi.org/10.3389/fimmu.2012.00211.

14. Bacchetta, R., and Roncarolo, M.G. (2024). IPEX syndrome from diagnosis to cure, learning along the way. J. Allergy Clin. Immunol. *153*, 595–605. https://doi.org/10.1016/j.jaci.2023.11.021.

15. Barzaghi, F., Amaya Hernandez, L.C., Neven, B., Ricci, S., Kucuk, Z.Y., Bleesing, J.J., Nademi, Z., Slatter, M.A., Ulloa, E.R., Shcherbina, A., et al. (2018). Long-term follow-up of IPEX syndrome patients after different therapeutic strategies: An international multicenter retrospective study. J. Allergy Clin. Immunol. *141*, 1036–1049.e5. https://doi.org/10.1016/j.jaci.2017.10.041.

16. Kawai, T., Saito, M., Nishikomori, R., Yasumi, T., Izawa, K., Murakami, T., Okamoto, S., Mori, Y., Nakagawa, N., Imai, K., et al. (2012). Multiple reversions of an IL2RG mutation restore T cell function in an X-linked severe combined immunodeficiency patient. J. Clin. Immunol. *32*, 690–697. https://doi.org/10.1007/s10875-012-9684-1.

17. Davis, B.R., Yan, Q., Bui, J.H., Felix, K., Moratto, D., Muul, L.M., Prokopishyn, N.L., Blaese, R.M., and Candotti, F. (2010). Somatic mosaicism in the Wiskott-Aldrich syndrome: molecular and functional characterization of genotypic revertants. Clin. Immunol. *135*, 72–83. https://doi.org/10.1016/j.clim.2009.12.011.

18. Miyazawa, H., and Wada, T. (2021). Reversion Mosaicism in Primary Immunodeficiency Diseases. Front. Immunol. *12*, 783022. https://doi.org/10.3389/fimmu.2021.783022.

19. Duclaux-Loras, R., Charbit-Henrion, F., Neven, B., Nowak, J., Collardeau-Frachon, S., Malcus, C., Ray, P.F., Moshous, D., Beltrand, J., Goulet, O., et al. (2018). Clinical Heterogeneity of Immune Dysregulation, Polyendocrinopathy, Enteropathy, X-Linked Syndrome: A French Multicenter Retrospective Study. Clin. Transl. Gastroenterol. *9*, 201. https://doi.org/10.1038/s41424-018-0064-x.

20. Jamee, M., Zaki-Dizaji, M., Lo, B., Abolhassani, H., Aghamahdi, F., Mosavian, M., Nademi, Z., Mohammadi, H., Jadidi-Niaragh, F., Rojas, M., et al. (2020). Clinical, Immunological, and Genetic Features in Patients with Immune Dysregulation, Polyendocrinopathy, Enteropathy, X-linked (IPEX) and IPEX-like Syndrome. J. Allergy Clin. Immunol. Pract. *8*, 2747–2760.e7. https://doi.org/10.1016/j.jaip.2020.04.070.

21. Kim, J.A., Cho, K., Shin, M.S., Lee, W.G., Jung, N., Chung, C., and Chang, J.K. (2008). A novel electroporation method using a capillary and wire-type electrode. Biosens. Bioelectron. *23*, 1353–1360. https://doi.org/10.1016/j.bios.2007.12.009.

22. Bindl, L., Torgerson, T., Perroni, L., Youssef, N., Ochs, H.D., Goulet, O., and Ruemmele, F.M. (2005). Successful use of the new immune-suppressor sirolimus in IPEX (immune dysregulation, polyendocrinopathy, enteropathy, X-linked syndrome). J. Pediatr. *147*, 256–259. https://doi.org/10.1016/j.jpeds.2005.04.017.

23. Passerini, L., Barzaghi, F., Curto, R., Sartirana, C., Barera, G., Tucci, F., Albarello, L., Mariani, A., Testoni, P.A., Bazzigaluppi, E., et al. (2020). Treatment with rapamycin can restore regulatory T-cell function in IPEX patients. J. Allergy Clin. Immunol. *145*, 1262–1271.e13. https://doi.org/10.1016/j.jaci.2019.11.043.

24. Xu, J., Winkler, J., Sabarinath, S.N., and Derendorf, H. (2008). Assessment of the impact of dosing time on the pharmacokinetics/pharmacodynamics of prednisolone. AAPS J. *10*, 331–341. https://doi.org/10.1208/s12248-008-9038-3.

25. Bevacqua, M., Baldo, F., Pastore, S., Valencic, E., Tommasini, A., Maestro, A., Rabusin, M., Arbo, A., and Barbi, E. (2019). Off-Label Use of Sirolimus and Everolimus in a Pediatric Center: A Case Series and Review of the Literature. Paediatr. Drugs *21*, 185–193. https://doi.org/10.1007/s40272-019-00337-7.

26. Baud, O., Goulet, O., Canioni, D., Le Deist, F., Radford, I., Rieu, D., Dupuis-Girod, S., Cerf-Bensussan, N., Cavazzana-Calvo, M., Brousse, N., et al. (2001). Treatment of the immune dysregulation, polyendocrinopathy, enteropathy, X-linked syndrome (IPEX) by allogeneic bone marrow transplantation. N. Engl. J. Med. *344*, 1758–1762. https://doi.org/10.1056/NEJM200106073442304.

27. Wang, J., and Metheny, L. (2023). Umbilical cord blood derived cellular therapy: advances in clinical development. Front. Oncol. *13*, 1167266. https://doi.org/10.3389/fonc.2023.1167266.

28. Brunstein, C.G., Miller, J.S., Cao, Q., McKenna, D.H., Hippen, K.L., Curtsinger, J., Defor, T., Levine, B.L., June, C.H., Rubinstein, P., et al. (2011). Infusion of ex vivo expanded T regulatory cells in adults transplanted with umbilical cord blood: safety profile and detection kinetics. Blood *117*, 1061–1070. https://doi.org/10.1182/blood-2010-07-293795.

29. Singh, S., Homad, L.J., Akins, N.R., Stoffers, C.M., Lackhar, S., Malhi, H., Wan, Y.H., Rawlings, D.J., and McGuire, A.T. (2020). Neutralizing Antibodies Protect against Oral Transmission of Lymphocryptovirus. Cell Rep. Med. *1*, 100033. https://doi.org/10.1016/j.xcrm.2020.100033.

30. Du, J., Wang, Q., Yang, S., Chen, S., Fu, Y., Spath, S., Domeier, P., Hagin, D., Anover-Sombke, S., Haouili, M., et al. (2022). FOXP3 exon 2 controls T(reg) stability and autoimmunity. Sci. Immunol. *7*, eabo5407. https://doi.org/10.1126/sciimmunol.abo5407.

31. Sato, Y., Liu, J., Lee, E., Perriman, R., Roncarolo, M.G., and Bacchetta, R. (2021). Co-Expression of FOXP3FL and FOXP3Delta2 Isoforms Is Required for Optimal Treg-Like Cell Phenotypes and Suppressive Function. Front. Immunol. *12*, 752394. https://doi.org/10.3389/fimmu.2021.752394.

32. Borna, S., Lee, E., Sato, Y., and Bacchetta, R. (2022). Towards gene therapy for IPEX syndrome. Eur. J. Immunol. *52*, 705–716. https://doi.org/10.1002/eji.202149210.

33. Borna, S., Meffre, E., and Bacchetta, R. (2024). FOXP3 deficiency, from the mechanisms of the disease to curative strategies. Immunol. Rev. *322*, 244–258. https://doi.org/10.1111/imr.13289.

34. Borna, Š., Lee, E., Nideffer, J., Ramachandran, A., Wang, B., Baker, J., Mavers, M., Lakshmanan, U., Narula, M., Garrett, A.K.H., et al. (2023). Identification of unstable regulatory and autoreactive effector T cells that are expanded in patients with FOXP3 mutations. Sci. Transl. Med. *15*, eadg6822. https://doi.org/10.1126/scitranslmed.adg6822.

35. MacMillan, M.L., Hippen, K.L., McKenna, D.H., Kadidlo, D., Sumstad, D., DeFor, T.E., Brunstein, C.G., Holtan, S.G., Miller, J.S., Warlick, E.D., et al. (2021). First-in-human phase 1 trial of induced regulatory T cells for graft-versus-host disease prophylaxis in HLA-matched siblings. Blood Adv. *5*, 1425–1436. https://doi.org/10.1182/bloodadvances.2020003219.

36. Sato, Y., Passerini, L., Piening, B.D., Uyeda, M.J., Goodwin, M., Gregori, S., Snyder, M.P., Bertaina, A., Roncarolo, M.G., and Bacchetta, R. (2020). Human-engineered Treg-like cells suppress FOXP3-deficient T cells but preserve adaptive immune responses in vivo. Clin. Transl. Immunol. *9*, e1214. https://doi.org/10.1002/cti2.1214.

37. Du, W., Noyan, F., McCallion, O., Drosdek, V., Kath, J., Glaser, V., Fuster-Garcia, C., Yang, M., Stein, M., Franke, C., et al. (2025). Gene editing of CD3 epsilon to redirect regulatory T cells for adoptive T cell transfer. Mol. Ther. *33*, 997–1013. https://doi.org/10.1016/j.ymthe.2025.01.045.

38. Shy, B.R., Vykunta, V.S., Ha, A., Talbot, A., Roth, T.L., Nguyen, D.N., Pfeifer, W.G., Chen, Y.Y., Blaeschke, F., Shifrut, E., et al. (2023). High-yield genome engineering in primary cells using a hybrid ssDNA repair template and small-molecule cocktails. Nat. Biotechnol. *41*, 521–531. https://doi.org/10.1038/s41587-022-01418-8.

39. Xie, K., Starzyk, J., Majumdar, I., Wang, J., Rincones, K., Tran, T., Lee, D., Niemi, S., Famiglietti, J., Suter, B., et al. (2025). Efficient non-viral immune cell engineering using circular single-stranded DNA-mediated genomic integration. Nat. Biotechnol. *43*, 1821–1832. https://doi.org/10.1038/s41587-024-02504-9.

40. Nitulescu, A.M., Du, W., Glaser, V., Kath, J., Aird, E.J., Cullot, G., Greensmith, R., Mikkelsen, N.S., Stein, M., Bak, R.O., et al. (2025). Single-stranded HDR templates with truncated Cas12a-binding sequences improve knock-in efficiencies in primary human T cells. Mol. Ther. Nucleic Acids *36*, 102568. https://doi.org/10.1016/j.omtn.2025.102568.

41. Sather, B.D., Romano Ibarra, G.S., Sommer, K., Curinga, G., Hale, M., Khan, I.F., Singh, S., Song, Y., Gwiazda, K., Sahni, J., et al. (2015). Efficient modification of CCR5 in primary human hematopoietic cells using a megaTAL nuclease and AAV donor template. Sci. Transl. Med. *7*, 307ra156. https://doi.org/10.1126/scitranslmed.aac5530.

42. Cooke, K.R., Kobzik, L., Martin, T.R., Brewer, J., Delmonte, J., Jr., Crawford, J.M., and Ferrara, J.L. (1996). An experimental model of idiopathic pneumonia syndrome after bone marrow transplantation: I. The roles of minor H antigens and endotoxin. Blood *88*, 3230–3239.

43. Snijder, J., Ortego, M.S., Weidle, C., Stuart, A.B., Gray, M.D., McElrath, M.J., Pancera, M., Veesler, D., and McGuire, A.T. (2018). An Antibody Targeting the Fusion Machinery Neutralizes Dual-Tropic Infection and Defines a Site of Vulnerability on Epstein-Barr Virus. Immunity *48*, 799–811.e9. https://doi.org/10.1016/j.immuni.2018.03.026.

YMTHE, Volume *34*

Supplemental Information

Preclinical efficacy and safety assessment of engineered regulatory T cells for treatment of IPEX and other autoimmune disorders

Yuchi Honaker, Noelle P. Dahl, Swati Singh, Akhilesh K. Singh, Christina Lopez, David Gruber, Samuel C. Scharffenberger, Shivani Patel, Harold Jones, Iram F. Khan, Michelle L. Christian, Su Jung Yang, Karen Sommer, Troy R. Torgerson, Eric J. Allenspach, Cade Ellis K. Ito, Gene I. Uenishi, Gregory J. Cost, Peter J. Cook, and David J. Rawlings

Supplemental Methods

Guide-seq and amplicon-seq analysis

Activated CD4$^+$ T cells were electroporated with Cas9/T9 gRNA RNP and 1 µM of dsODN[1] using Lonza 4D Nucleofector. As a background control, cells were only transfected with the same amount of dsODN to capture Cas9-independent DNA double strand break. Genomic DNA was extracted from transfected T cells 2-3 days after transfection for library preparation, next-generation sequencing (NGS) and data analysis following instructions described by Tsai et al.[1]

To perform amplicon seq analysis, CD4$^+$ T cells were transfected with Cas9 RNP complex consisting of either wild-type TrueCut Cas9 (Invitrogen) and sgRNA (Synthego) or Spyfi Cas9 (Aldeveron) and sgRNA (Biospring) as research grade and GMP grade reagents respectively. Genomic DNA was PCR amplified with primers designed to target the off-targets identified in guide-seq. Amplicons were then indexed (Nextera XT Index Kit (Illumina) and sequenced using MiSeq with, 2x150, 15M reads for each sample.

TCR repertoire analysis

Genomic DNA extracted from the EngTreg products and the CD4$^+$ T cells directly purified from autologous PBMCs without expansion were submitted for spectratyping analysis of TCR-beta chain (The Immune Monitoring Lab at Fred Hutch) or TCRbeta sequencing (Adaptive Biotechnologies). TCR sequences were assessed on their total proportion of unique TCR sequences using Immunarch (http://doi.org/10.5281/zenodo.3367200*)* R package and grouped by experiment and timepoint.[2] For experiments with replicates, a Wilcoxan rank sum test is used to compare between timepoints. Clonotype abundance of every TCR was then evaluated per experiment per timepoint and graphed.

Supplemental Tables

Table S1. Human *FOXP3* guide RNA target sequences. List of guide RNA target sequences tested. 20nt target sequence without PAM is shown.

GUIDE	TARGET SEQUENCE (5'->3')
T1	TTCCAGGGCCGAGATCTTCG
T3	CGCCTCGAAGATCTCGGCCC
T4	TCGAAGATCTCGGCCCTGGA
T7	GGCCCTGGAAGGTTCCCCCT
T9	TCCAGCTGGGCGAGGCTCCT
T18	TCAGACCTGCTGGGGGCCCG

Table S2. Oligonucleotide sequences. Full list of PCR primers and ddPCR probes used in the study.

NAME	SEQUENCE (5' -- 3')	EXPERIMENT
hFOXP3 NHEJ-F	CTCGGGACATGTCCCAGCCAATGC	PCR *FOXP3* nuclease cleavage site; Sequence integrated donor
hFOXP3 NHEJ-R	CTGCATAAGTCACAGACTTGCCTGGGAC	PCR *FOXP3* nuclease cleavage site
hFOXP3 HDR 2-F	GCTCAAGAGACCCCATCTCTCC	PCR amplify donor template within *FOXP3* target; binds outside of homology arms
hFOXP3 HDR 2-R	GCACATGTGGGCTGTGGTTCA	PCR amplify donor template within *FOXP3* target; binds outside of homology arms
LNGFR 3'HA seq-F	GTCTATTGCTCCATCCTGGCTG	sequence *FOXP3* integrated donor template
LNGFR 3'HA seq-R	GTGGGGTACCTGGACCTACAGGTG	sequence *FOXP3* integrated donor template
5'HA MND seq-F	CTCGGGACATGTCCCAGCCAATGC	sequence *FOXP3* integrated donor template
5'HA MND seq-R	GCAGTTTCTAGAGAACCATCAGATGTTTCC	sequence *FOXP3* integrated donor template
5'HA seq-F	CAGACTCTTCATGTCTATCTACACCTG	sequence *FOXP3* integrated donor template
5'HA seq 2-F	GGACACATCCACACCAGGGCTG	sequence *FOXP3* integrated donor template
5'HA seq 3-F	CATCCAAGCTGCTAGCACTGC	sequence *FOXP3* integrated donor template
3'HA seq-R	CTAGTCATGGTGGCACCCTC	sequence *FOXP3* integrated donor template
ddPCR Insert-F	GGCACCTCCAGAACAAGACC	ddPCR amplify FOXP3 with integrated donor template; binds to donor template
ddPCR Insert-R	TCCTGATCCTCACTGTTCTGTGTC	ddPCR amplify FOXP3 with integrated donor template; binds downstream of donor template
ddPCR Control-F	GTTCACACGCATGTTTGCCT	ddPCR amplify an unedited region of FOXP3; binds downstream of donor template
ddPCR Control-R	ATCCTGAGGGTACTGACGCT	ddPCR amplify an unedited region of FOXP3; binds downstream of donor template
ddPCR Insert Probe-FAM	AGACCCACAACCACAGCAGC	ddPCR probe for quantification of target DNA; binds within FOXP3 integrated donor template
ddPCR Control Probe-HEX	TGGCGGTGACTGGGATGGC	ddPCR probe for quantification of target DNA; binds to an unedited region of FOXP3

Table S3. Flow Cytometry Antibodies. Full list of Flow Cytometry antibodies used in the study.

ANTIGEN	ANTIBODY	VENDOR	CATALOG#	CLONE
		ANTIBODY FOR HUMAN CELLS		
LNGFR	FITC anti-human LNGFR	Miltenyi biotec	130-113-420	ME20.4-1.H4
	APC anti-human LNGFR	Miltenyi biotec	130-113-418	ME20.4-1.H4
	PE anti-human LNGFR	Miltenyi biotec	130-113-421	ME20.4-1.H4
CD235a	Pacific Blue™ anti-human CD235a (Glycophorin A)	BioLegend	349108	HI264
CD127	PE-CF594 anti-human CD127	BD Biosciences	562397	HIL-7R-M21
	BV510 Mouse Anti-Human CD127	BD Biosciences	563086	HIL-7R-M21
LAG3	BV421 anti-human LAG3	BioLegend	369314	11C3C65
ICOS	AF700 anti-human ICOS	BioLegend	313528	C398.4A
FOXP3	PE anti-human FOXP3	BioLegend	320208	259D
CTLA-4	APC anti-human CTLA-4	BioLegend	349908	L3D10
CD40L	PE anti-human CD40L	BD Biosciences	555700	TRAP-1
CD69	BV605 anti-human CD69	BioLegend	310937	FN50
HELIOS	PE-Cy7 anti-human HELIOS	BioLegend	137236	22F6
	BV610 anti-human HELIOS	Thermo Fisher	50-112-4891	22F6
CD25	PE-Cy7 anti-human CD25	BD Biosciences	335789	2A3
	PE anti-human CD25	BD Biosciences	341009	2A3
	BV650 anti-human CD25	BD Biosciences	563719	M-A251
CD4	PerCP-Cy5.5 anti-human CD4	BioLegend	300530	RPA-T4
	FITC-anti-human CD4	BD Biosciences	555346	RPA-T4
	Alexa700 anti-human CD4	BD Biosciences	557922	RPA-T4
	BV711 anti-human CD4	BD Biosciences	563028	SK3
CD3	eFluor 450 anti-human CD3	Thermo Fisher	48-0037-42	OKT3
	BV510 anti-human CD3	BD Biosciences	740202	SK7
	BV421 Mouse Anti-human CD3	BD Biosciences	563797	SK7
IFN-γ	AF647 anti-human IFN-γ	BioLegend	502516	4S.B3
TNF-α	APC-Cy7 anti-human TNF- α	BioLegend	502944	MAb11
IL-2	PE-Cy7 anti-human IL-2	Thermo Fisher	50-112-9499	MQ1-17H12
LAP	PerCP-Cy5.5 anti-human LAP	BD Biosciences	562544	TW4-2F8
IL-4	BV421 anti-human IL-4	BioLegend	500826	MP4-25D2
IL-17A	AF700 anti-human IL-17A	BD Biosciences	560613	N49-653
CD69	BV605 anti-human CD69	BioLegend	310937	FN50
CD8	PerCP-Cy5.5 anti-human CD8	BD Biosciences	560662	RPA-T8
	PE anti-human CD8	Life Technologies	No.50-101-93	SK1
CD137	BV421 Anti-human CD137	BD Biosciences	564091	4B4-1
CD45	FITC anti human CD45	Fisher Scientific	5010066/11945941	2DA
CD45RO	PerCP-Cy5.5 anti-human CD45RO	BioLegend	304222	UCHL1
CD45RA	APC anti-human CD45RA	BD Biosciences	561210	5H9
CD33	PE anti-human CD33	BD Biosciences	555450	WM53
CD19	PE-Cy7 anti-human CD19	Fisher Scientific	501129016/25019942	HIB19
CD38	PerCP-Cy5.5 anti-human CD38	BD Biosciences	551400	HIT2
CD24	BV605 anti-human CD24	BioLegend	311123	ML5
IgM	Pacific blue anti-human IgM	BioLegend	314514	MHM-88

IgD	Biotin anti-human IgD	BD Biosciences	555777	IA6-2
Streptavidin	PE-Streptavidin	BD Biosciences	554061	N/A
CD4	Ultra-LEAF™ Purified anti-human CD4 Antibody	BioLegend	317404	OKT4
CD8	CD8a Mouse anti-human, Functional Grade	Fisher Scientific	5014218	OKT8
		ANTIBODY FOR MURINE CELLS		
ANTIGEN	**ANTIBODY**	**VENDOR**	**CATALOG#**	**CLONE**
LNGFR	CD271 (LNGFR) anti-human/mouse	Miltenyi Biotec	130125199	REA648
CD25	PE anti-mouse CD25	Thermo Fisher	**12-0251-82**	PC61.5
CD19	Alexa Fluor 700 mouse CD19	BD Biosciences	557958	1D3
mCD4	BV785 anti-mouse CD4	BioLegend	100453	GK1.5
CD45.1	PerCP-Cy5.5 anti-mouse CD45.1	Thermo Fisher	50-157-98	A20
CD45.2	APC anti-mouse CD45.2	Thermo Fisher	50-149-79	104
CD45	PerCP-Cy5.5 anti-mouse CD45	BioLegend	103132	30F-11
	BV421 anti-mouse CD45	Fisher Scientific	501129701 /48045182	30F-11
Live/Dead	eFluor 780 fixable viability dye	Fisher Scientific	50-169-66	N/A
CD8	PE-Cy7 anti-mouse CD9	BioLegend	100722	53-6.7
B220	BV421 anti-mouse B220	BioLegend	103239	RA3-6B2

Table S4. Scoring criteria for Xeno-GvHD studies. Phenotypic scoring guide for determining humane endpoint in Xeno-GvHD mouse studies.

Criteria	**Grade 0**	**Grade 1**	**Grade 2**
Weight Loss	<10%	>10% to <20%	>20%
Posture	Normal	Hunching noted only at rest	Severe hunching impairs movement
Activity	Normal	Mild to moderately decreased	Stationary unless stimulated
Fur Texture	Normal	Mild to moderate ruffling	Severe ruffling/poor grooming
Skin Integrity	Normal	Scaling of paws/tail	Obvious areas of denuded skin

A

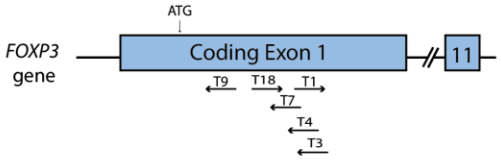

B

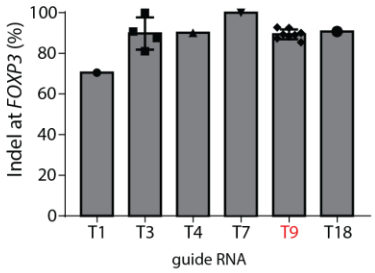

C

T9 guide RNA In-Silico Off-Target prediction

Coordinates	Strand	MM	Target Seq	PAM	Distance	Region	Gene Name
chrX:49258427-49258449	+	0	TCCAGCTG[GGCGAGGCTCCT]	GGG	0	Exonic	FOXP3
chrX:346300-346322	-	4	CCGTGCGG[GGCGAGGCTCCT]	GGG	0	Exonic	PPP2R3B
chr1:19683304-19683326	+	4	TGCTGCCT[GGCGAGGCTCCT]	CGG	0	Exonic	TMCO4
chr12:48856424-48856446	-	4	CAAAGCTG[GGGGAGGCTCCT]	GGG	699	Intergenic	RND1
chr11:116179067-116179089	-	3	TGGAGCTG[GGCAAGGCTCCT]	GGG	N/A	N/A	N/A
chr10:25016920-25016942	+	4	TGCTTCTG[GTCGAGGCTCCT]	CGG	131	Intronic	THNSL1
chr9:134785535-134785557	+	2	TCCAGCTG[TGGGAGGCTCCT]	GGG	438	Intronic	COL5A1

D

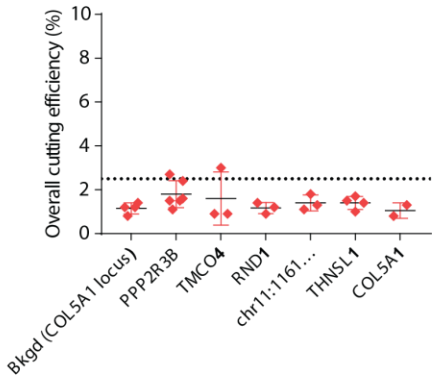

E

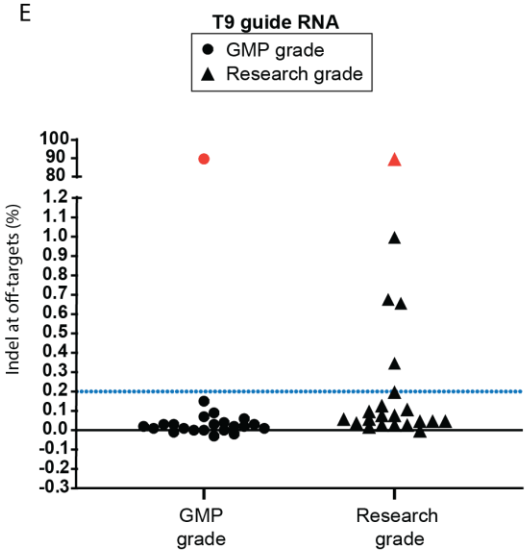

F

T9 guide RNA Target Site List

Off-target	Region	Gene or nearest gene	% Indel	
			Research	GMP
chr8_38778773	Intron	TACC1	0.99	0.04
chr2_95756122	Intergenic	TMEM182	0.19	0.03
chr9_130977101	Intergenic	DBH	0.1	-0.01
chr11_116179073	Intergenic	NCAM1	0.09	0.03
chr19_28839161	Intergenic	AC005394.2	0.65	0.09
chr2_96068320	Intergenic	CNNM4	0.12	0.06
chr12_114341837	Intron	PLBD2	0.02	0.01
chr1_15721130	Intron	PLEKHM2	0.05	0.03
chr15_85792818	Intron	KLHL25	0.04	0
chr8_132054216	Intron	OC90	0.07	0
chr21_41562401	Intron	AP001610.3	0.04	0.01
chr15_74606268	Exon	CLK3	0.04	-0.02
chr15_74385407	Intron	LINC02255	0.03	0.02
chr15_90351589	Intergenic	FANCI	-0.01	-0.03
chr7_149293591	Intron	ZNF783	0.02	0.02
chr4_499278	Exon	PIGG	0.34	0.01
chr19_28839170	Intergenic	LINC00906	0.67	0.15
chr22_19882185	Intron	TXNRD2	0.02	0.03
chr2_60498373	Intron	BCL11A	0.05	0.07
chr15_85792817	Intron	KLHL25	0.07	0.02
chr6_52995352	Intergenic	GSTA4	0.01	0

Figure S1. Development of human FOXP3 gene editing. (A) Annotations of guide RNAs designed to target the first coding exon of human FOXP3. (B) Insertion and deletion (Indel) analysis to determine on-target DNA cleavage efficiency of guide RNAs assembled in the CRISPR Cas9 RNP by colony sequencing, inference of CRISPR Edits (ICE) or ddPCR in human CD4+ T cells (mean ± SD). (C) Predicted in-silico off-targets for FOXP3 guide RNA T9 based on ccTOP CRISPR/Cas9 target predictor algorithm. (D) Overall cutting efficiency of T9 guide at predicted off-target sites based on ICE analysis. Graph (E) and target site list (F) of genome-wide off-target cleavage and indel analysis of cGMP-grade Cas9 and FOXP3-T9 guide RNA. Research grade materials were used as control. On-target cleavage is indicated in red shown in D.

A

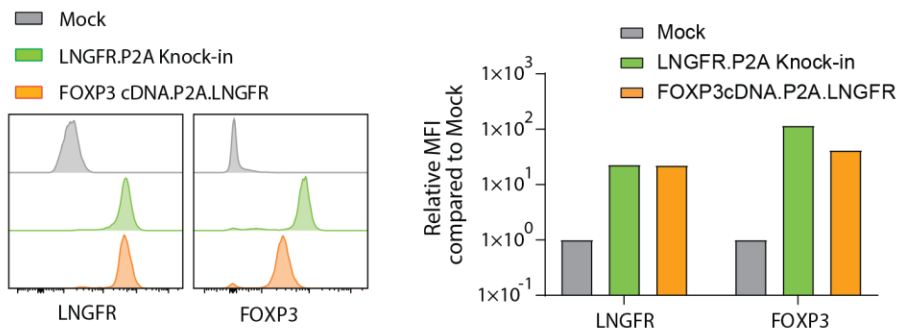

B

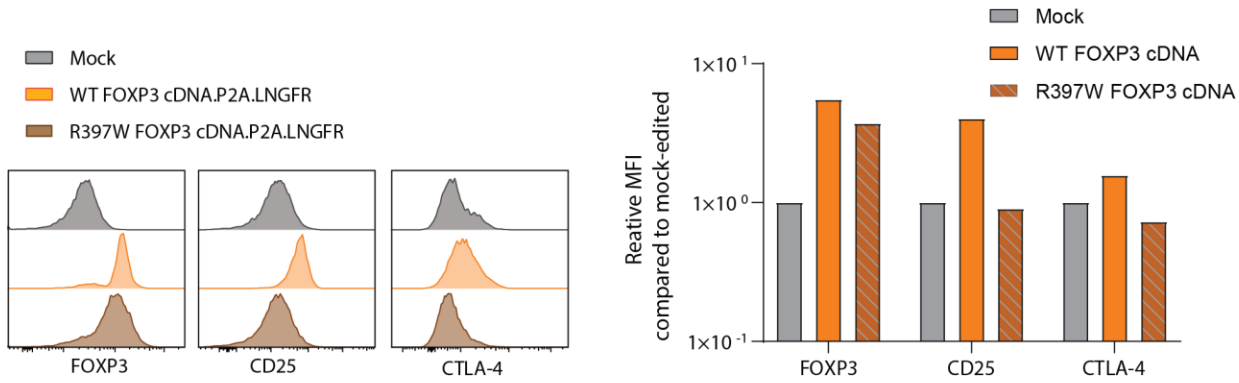

Figure S2. Immunophenotype of FOXP3 cDNA expressing EngTreg products. (A) Representative histograms (left) and relative MFI (right) showing expression levels of LNGFR marker and FOXP3 in mock-edited cells and EngTreg generated with MND.LNGFR.2A KI or MND. FOXP3cDNA.P2A.LNGFR. (B). Representative histograms (left) and MFI (right) showing expression levels of FOXP3, CD25, and CTLA-4 in mock-edited cells, and EngTreg expressing either WT or R397W FOXP3.

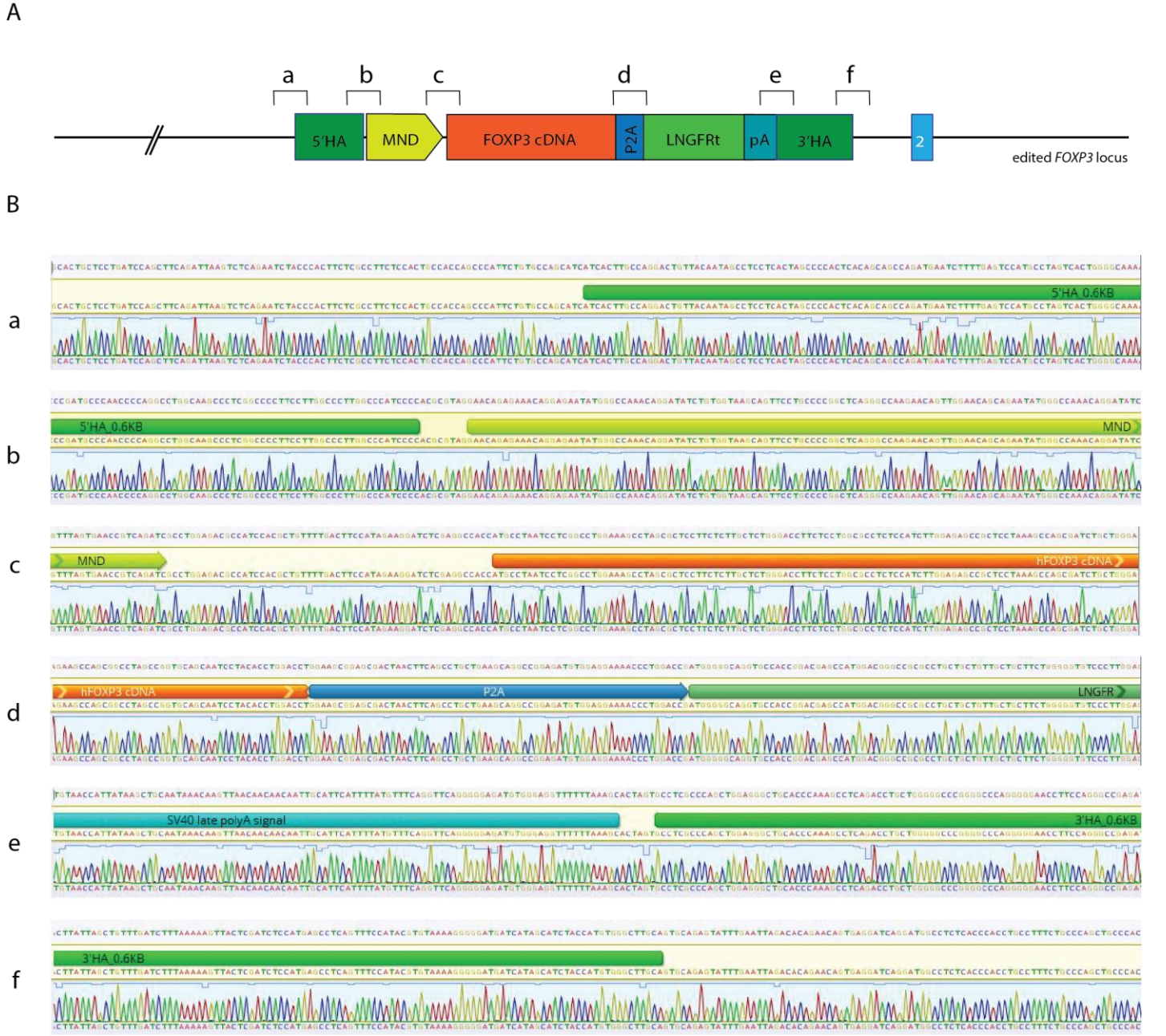

Figure S3. Seamless integration of repair template through HDR. (A) Schematic of the expected integration of the repair template to human FOXP3 locus by HDR. Genomic DNA isolated from the enriched and expanded EngTreg was PCR amplified using oligo pairs corresponding to upstream of 5' homology arm and downstream of 3' homology arm. The amplicons were then subjected to Sanger sequencing and alignment using Geneious software. (B) Portions of the alignment assembly (brackets a-f) shown. In each alignment, Sanger sequencing reads are shown as the bottom sequences and the chromatograms, with annotations shown in the middle, and the consensus sequences shown at the top.

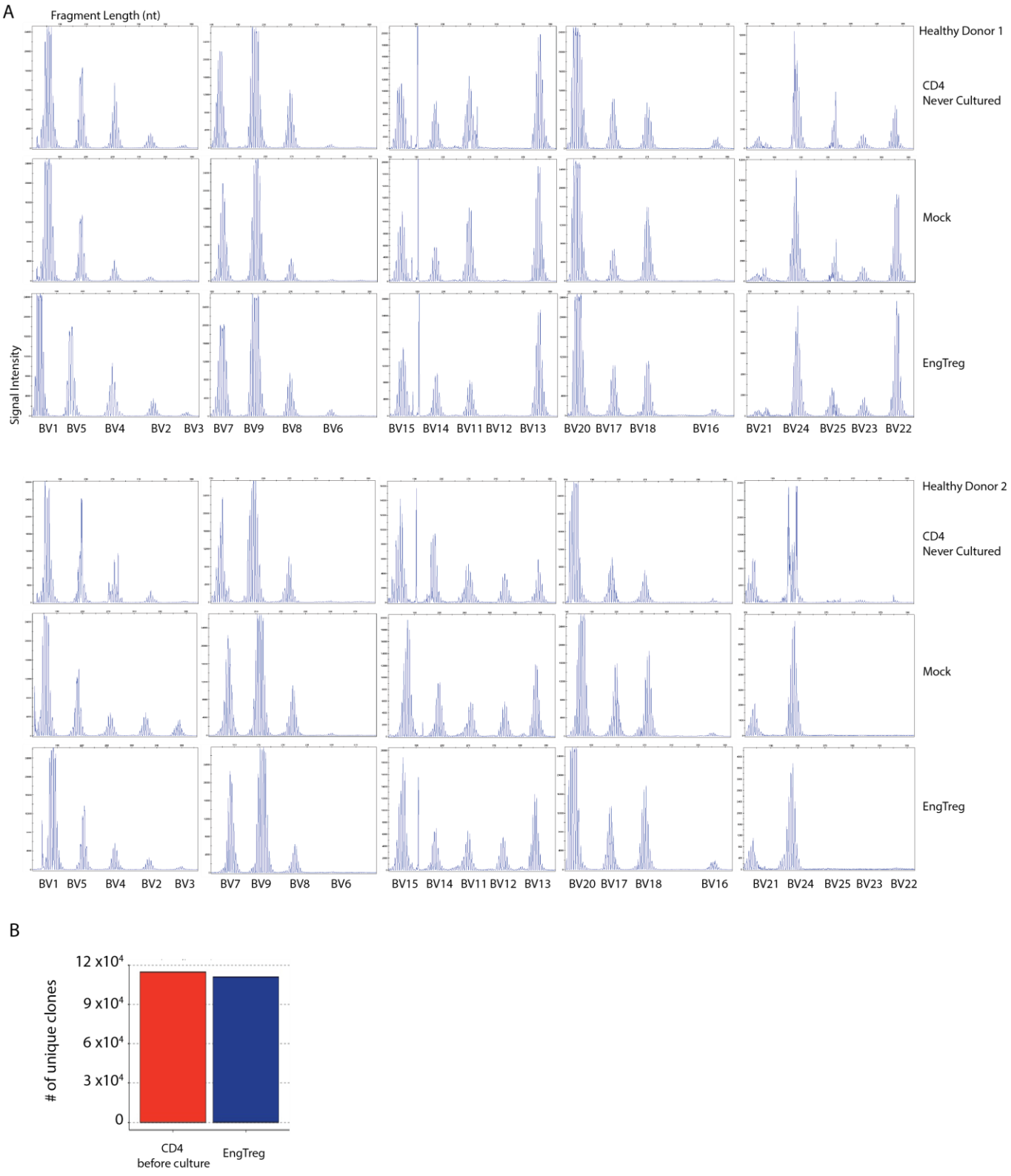

Figure S4. EngTreg retain TCR clonal diversity after in vitro engineering and expansion. (A) Representative data showing TCRb spectra-typing analysis of CD4+ T cells comparing: upper panels, T cells freshly isolated from donor-matched PBMC; middle panels, mock-edited T cells; and lower panels, HDR edited and expanded, EngTreg products from 2 healthy donors (n=3). (B) Adaptive TCR sequencing was also performed using one cell product to examine TCR clonality. Numbers of unique clones in EngTreg were compared to that of CD4+ cells isolated from autologous PBMCs without in vitro culture or expansion.

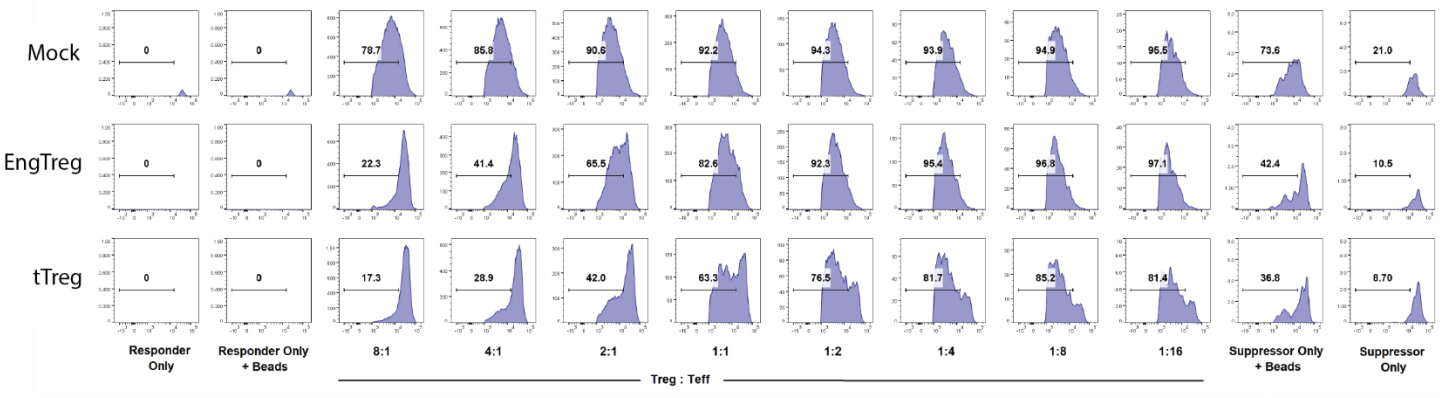

Figure S5. Proliferation of suppressor cells in T cell in-vitro suppression assay. Representative histograms for eFlour670 in Mock, EngTreg, and tTreg suppressor cell populations at day 4 of in-vitro suppression assay with CTV labeled polyclonal Teff target cells.

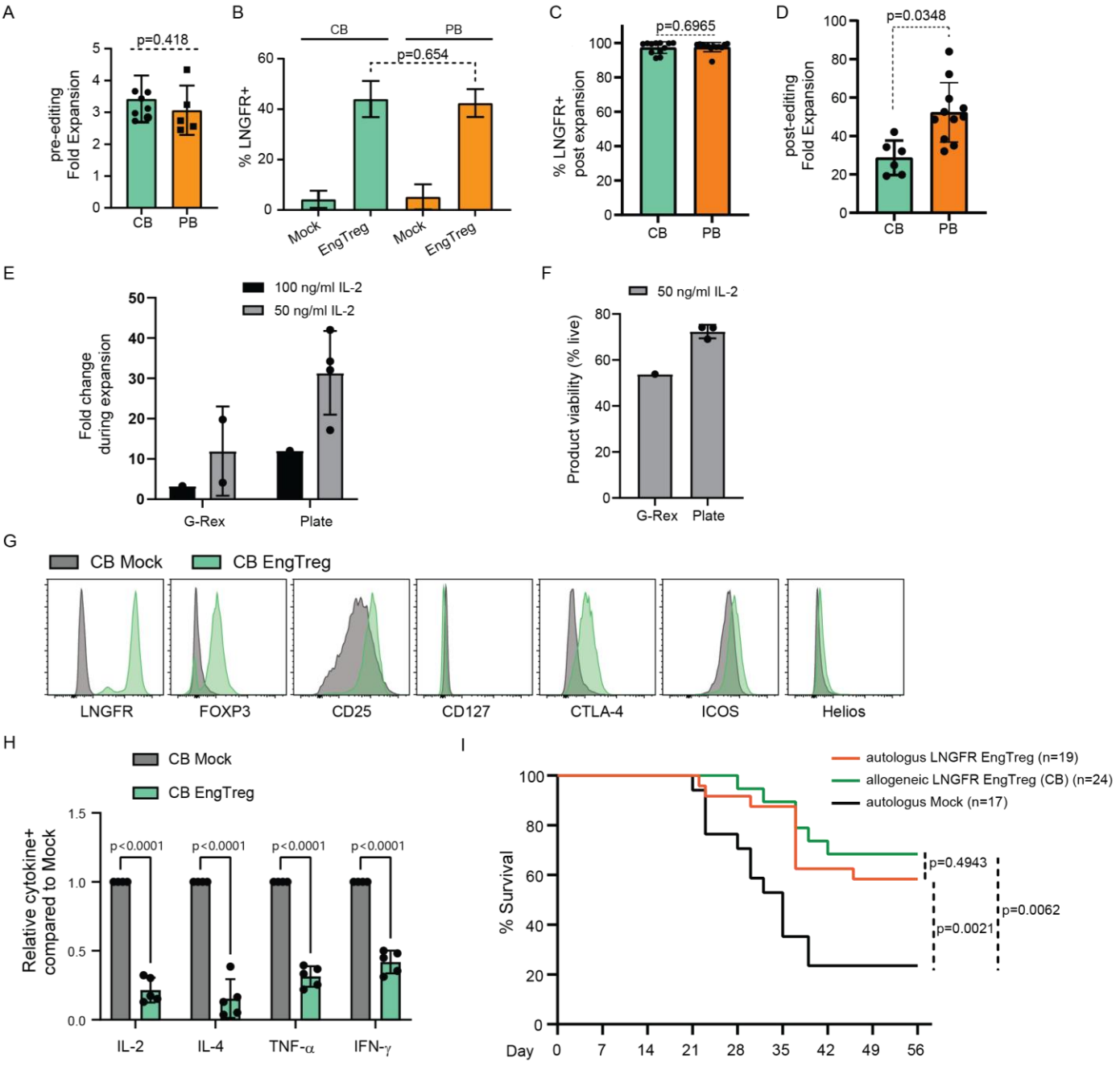

Figure S6. Generation of EngTreg from umbilical cord blood CD4+ T cells. (A) Fold expansion of cord blood (CB) and peripheral blood (PB)-derived CD4$^+$ T cells in response to CD3/CD28 bead activation prior to gene editing (mean ±SD, 7 CB donors, 5 PBC donors, p-values based on unpaired T-test). (B) Graph showing editing efficiency of CB and PB derived CD4$^+$ T cells measured by percent LNGFR at day 2 after editing (mean ±SD, 7 CB donors, 4 PBC donors, p-value based on unpaired T-test). (C) Cell product purity after a 7-day expansion of LNGFR-enriched edited cells. (D) Fold change in cell expansion post-editing at day 7. (E) Fold change during the expansion phase in G-rex or regular culture plates in the presence of 50 vs. 100 ng/ml IL-2. (F). Cell viability at end of expansion in G-rex or regular culture plates in the presence of 50 ng/ml IL-2. Percent live cell is determined by viability dye staining and flow cytometry. (G) Representative histograms show expression of LNGFR and Treg-associated markers in CB derived EngTreg. Mock-edited cells prepared in parallel were used as control. (H) Intracellular IL-2, IL-4, TNF-α, and IFN-γ in CB-derived EngTreg and mock-edited cells after PMA/Ionomycin stimulation (MFI data normalized to Mock, mean ±SD, n=5 CB donors, p-values based on unpaired T-test). (I) Survival curve of NSG mice in xenoGvHD study. Data presented are combined results of 2 CB cell products against 3 different allogenic PB-derived CD4$^+$ Teff cell products, respectively. Autologous PB derived EngTreg and mock-edited cells were included as controls. P-values calculated using Log-rank (Mantel-Cox) test.

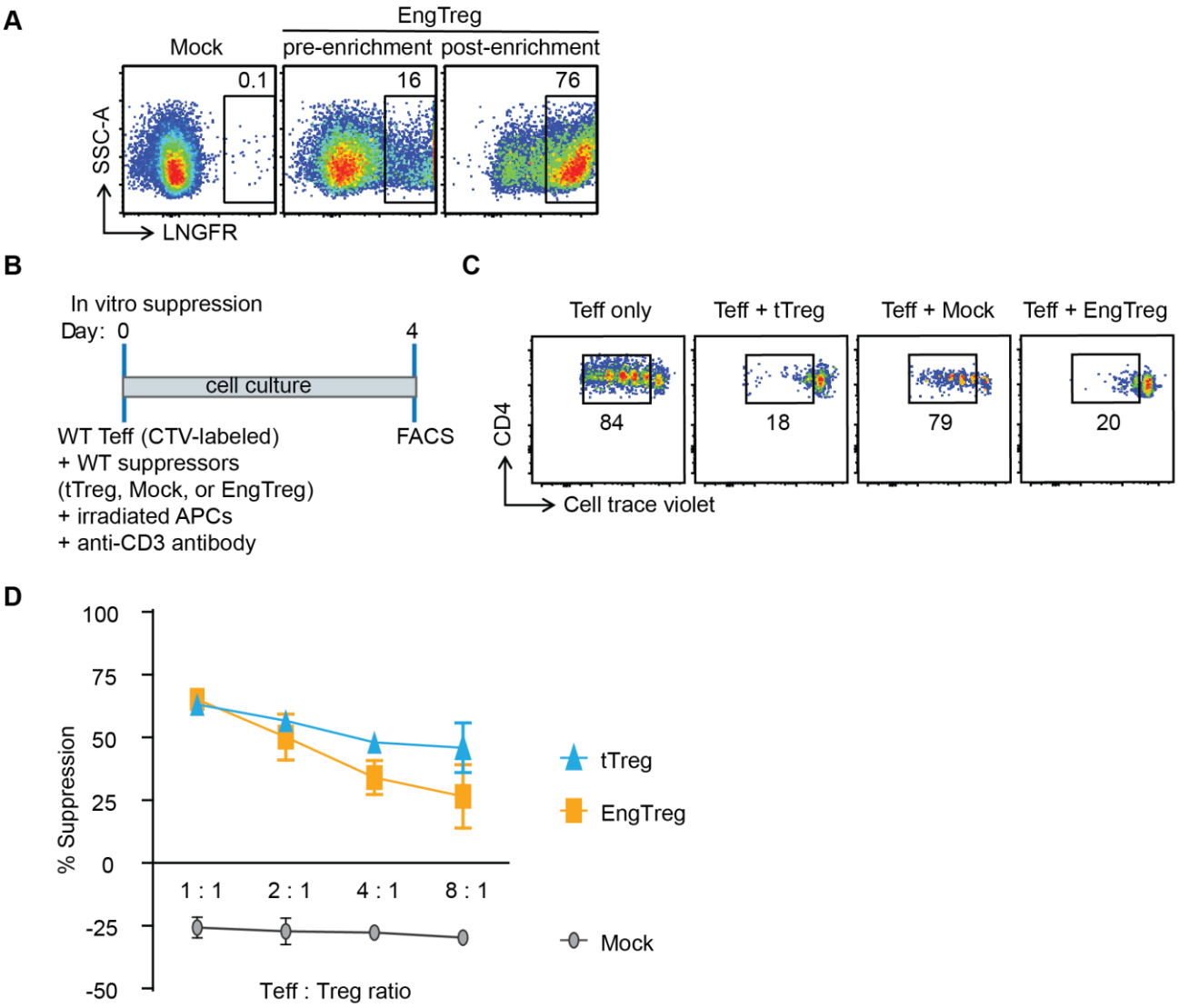

Figure S7. Generation of syngeneic murine EngTreg. (A) Flow plots showing LNGFR marker expressing population in control (mock-edited) and pre- (middle) and post-LNGFR enrichment (right) murine EngTreg. (B) Schematic of in vitro suppression assays performed using WT (C57BL/6) $CD4^+$ Teff cells and mock, tTreg or EngTreg cell products. (C) Representative flow plots (from one of two independent experiments) showing proliferation of CTV labeled $CD4^+$ Teff when co-cultured with the indicated cells after 4 days. (D) Graph showing the percent suppression of $CD4^+$ Teff proliferation by the indicated co-culture at varying ratios of Teff: Treg. % suppression = [100 - % normalized suppression]; % normalized suppression = 100/proliferation of Teff only condition × Teff proliferation in the presence of suppressor.

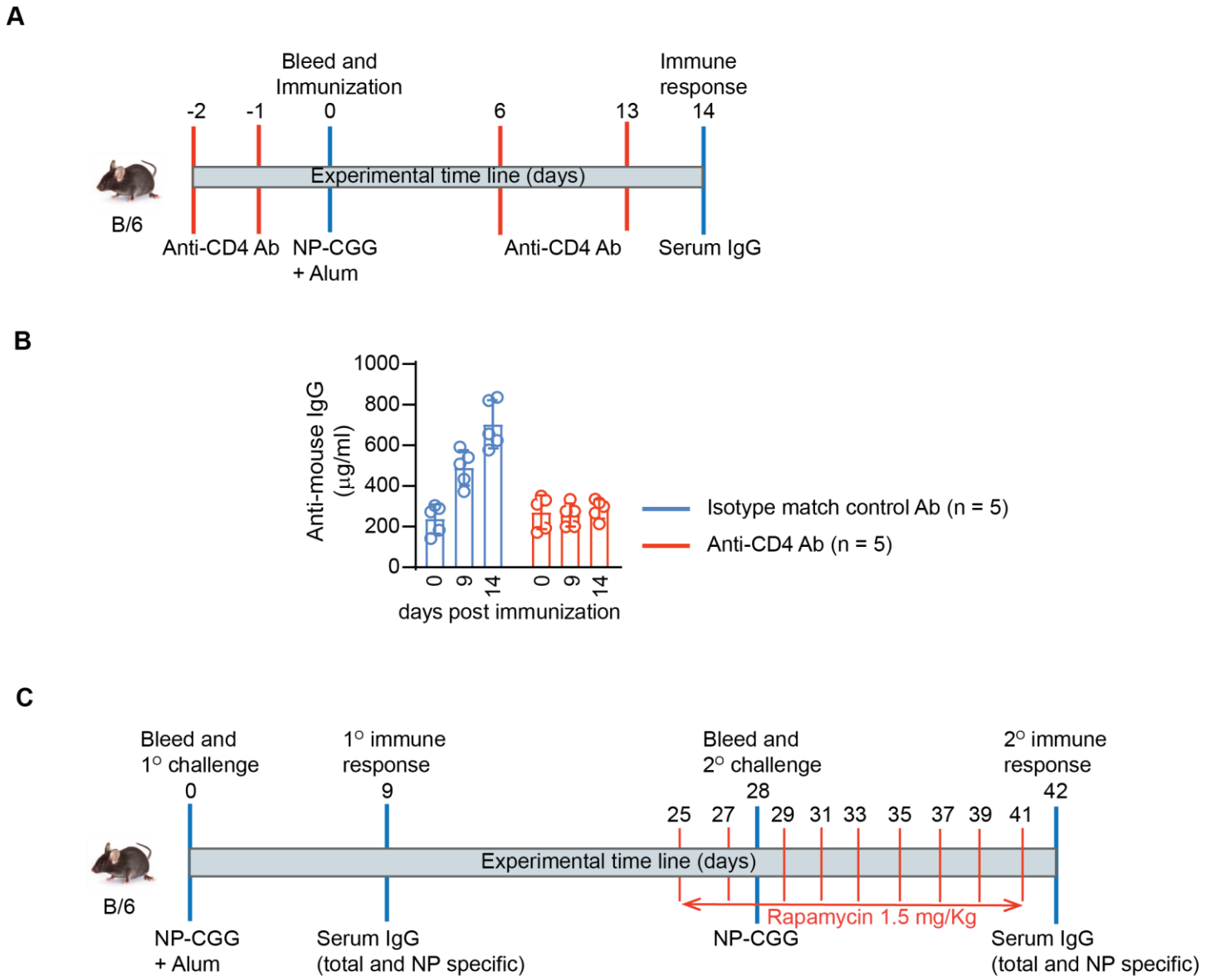

Figure S8. NP-CGG driven humoral immune response is dependent on T cell help. (A) Schematic showing the experimental timeline for NP-CGG driven primary antibody response in the presence or absence of $CD4^+$ T cells based on treatment with an anti-CD4 depleting antibody or an isotype control antibody. (B) Graph showing the serum titer of total IgG on days 0, 9, and 14 post immunization with NP-CGG (mean ±SD, n=5 per antibody treatment group). (C) Schematic showing the experimental timeline for treatment with rapamycin during humoral immune response upon secondary NP-CGG challenge.

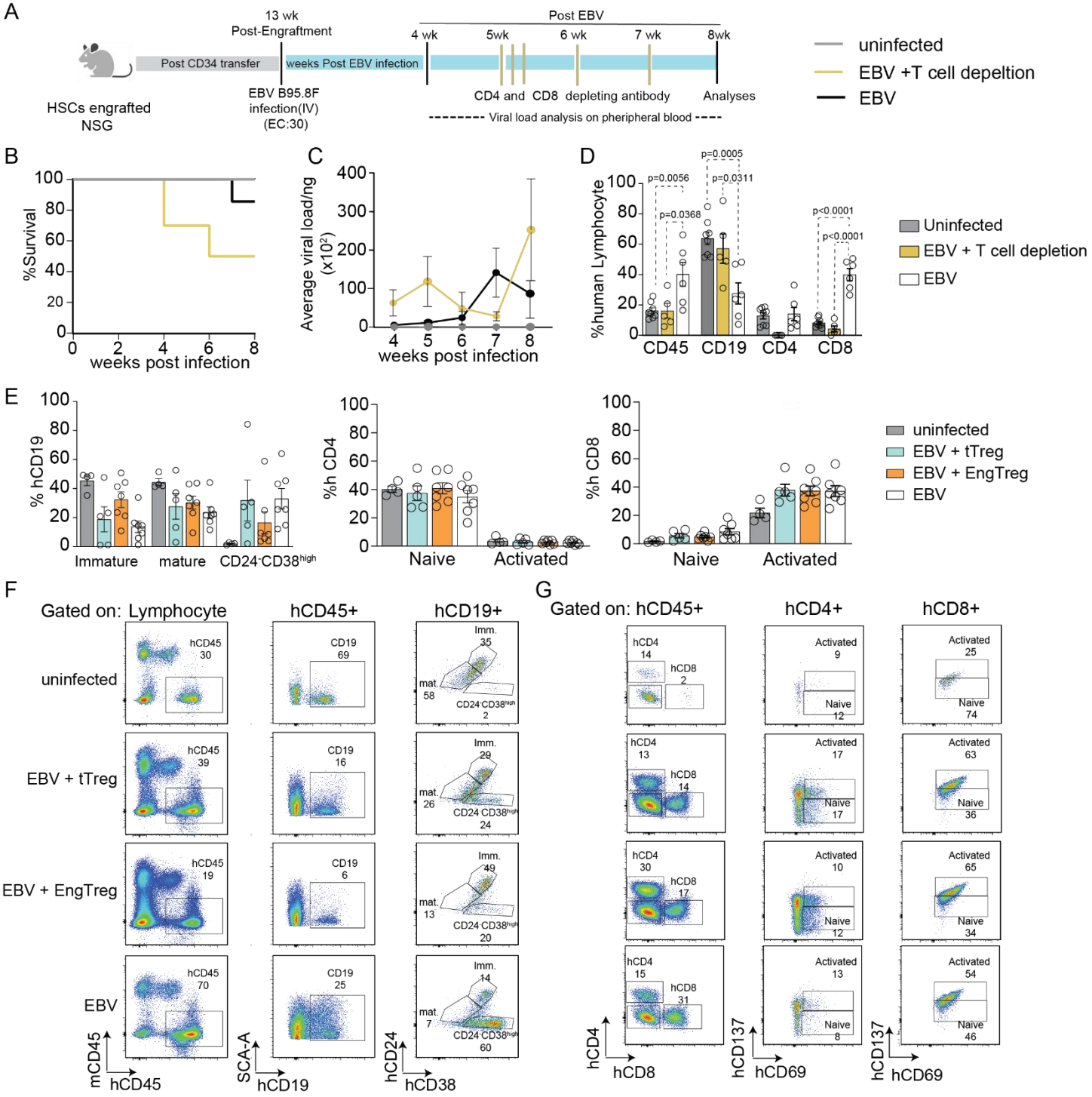

Figure S9. T dependent control of EBV infection in humanized NSG model is not impacted by the infusion of tTreg or EngTreg. (A) Schematic showing the experimental timeline for T cell depletion in humanized NSG mice infected with EBV. Starting at 5-week post EBV infection, mice were received intraperitoneal injections of anti-hCD4 and anti-hCD8 depleting antibodies as indicated. Peripheral blood was collected weekly between 4 to 8 weeks post infection to determine the viral load in circulation. Mouse spleens were analyzed at 8 weeks post infection for viral load and differentiation of human lymphocytes. (B) Survival curve of no-EBV infection group (n=8), EBV infection group (n=7), and EBV infection with T-cell depletion group (n=10). (C) EBV viral load quantification in peripheral blood by ddPCR (mean ±SD). (D) Frequency of differentiated human lymphocyte population in spleen (mean ±SD, n=8, 6, and 5 for no EBV infection group, EBV infection group and EVB infection with T-cell depletion, respectively). (E) $CD19^+$ B cell (left) and $CD4^+$ (middle) and $CD8^+$ T (right) cell subset differentiation in spleen (mean ±SD; n=3 uninfected control; n=4 EBV + tTreg; n=7 EBV + EngTreg; n=7 EBV only). Data shown is representative from one of 4 independent experiments. (F) and (G) Representative flow plots indicating gating strategy for human B cell and T cell subset analysis in mouse spleen. (F) hCD19 cells were gated from $hCD45^+$ and subsequently analyzed for expression of hCD24 and hCD38. $CD24^+CD38^{high}$ indicate the immature B subset, CD24low CD38 low indicate the mature B subset, while CD24-CD38high indicated B cells responsive to EBV infection. (G) $hCD4^+$ or $hCD8^+$ cells gated from hCD45+ cells were further analyzed for hCD69 and hCD137 to identify naïve ($CD69^+$ CD137-) and activated ($CD69^+CD137^+$) T cell subset populations. P-values calculated based on unpaired T test.

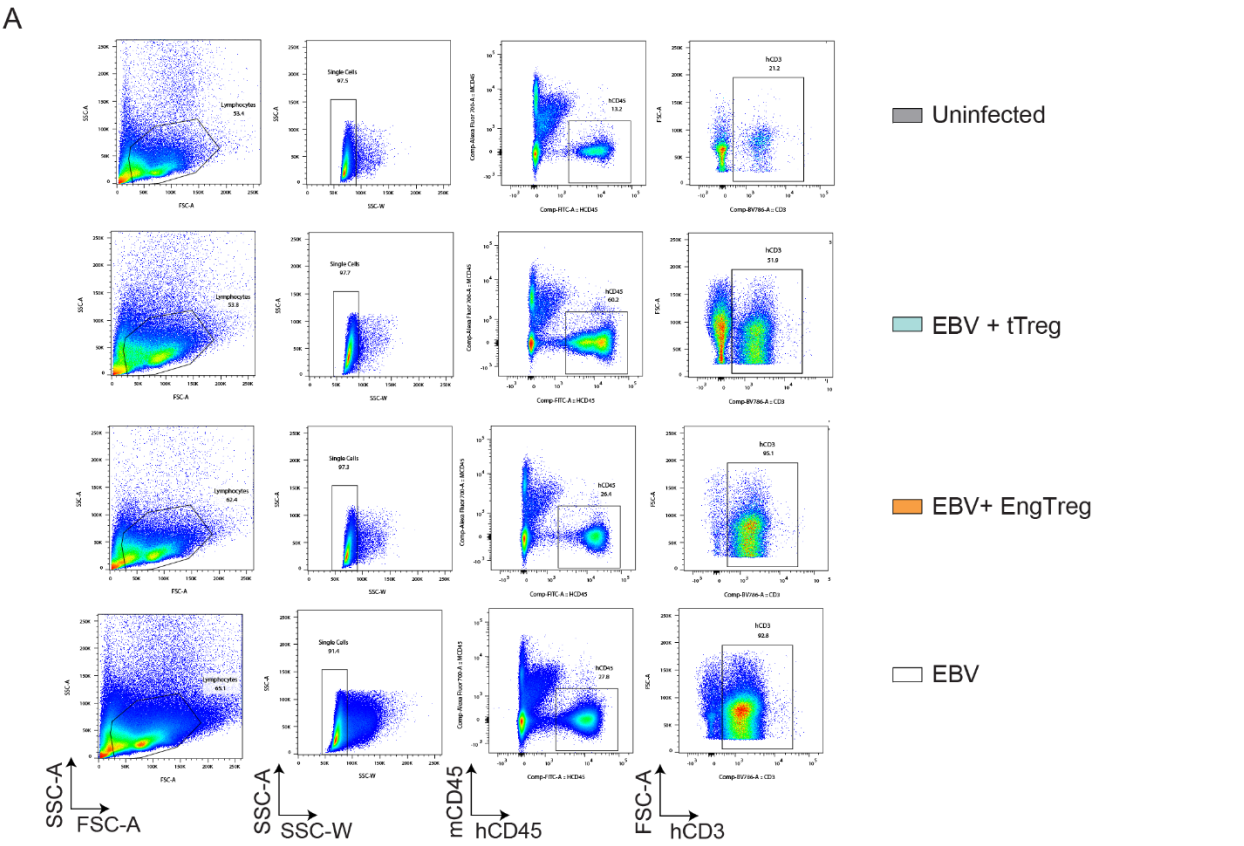

Figure S10. T cell populations in EBV-infected humanized mice treated with Treg. (A) Representative flow cytometry plots from spleen for humanized mice from indicated treatment groups. Graphed data for percent human CD3 (of human CD45^{+}) (B) and human FOXP3 (of human CD4^{+}) (C). Graphed data represents mean +/- SEM. P-value based on unpaired T test.

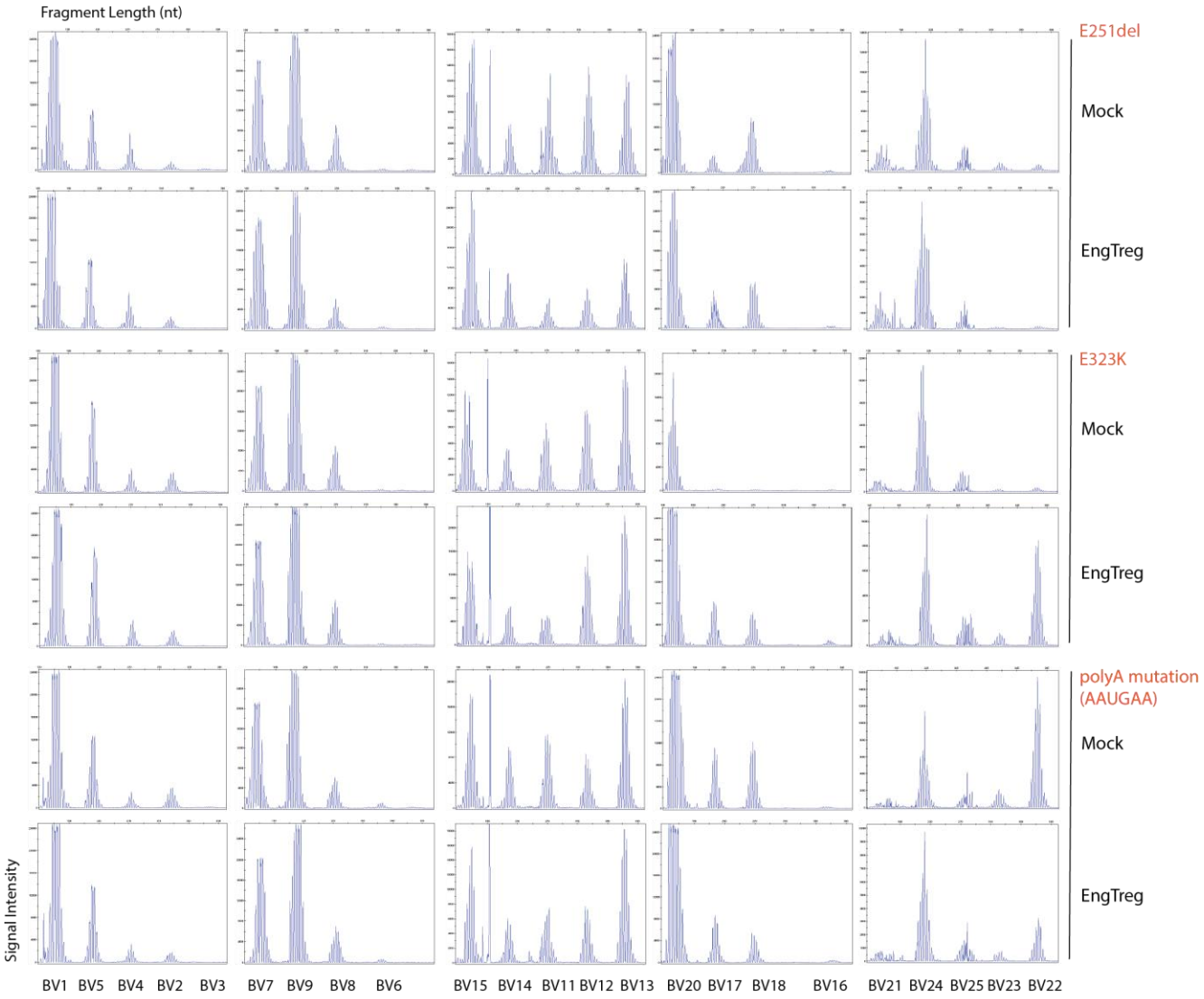

Figure S11. TCR diversity of EngTregs derived from IPEX patients. TCRb spectratyping results for EngTreg vs. mock-edited T cell products derived from IPEX patients with E251del, E323K, or poly A signal mutation.

References

1. Tsai, S.Q., Zheng, Z., Nguyen, N.T., Liebers, M., Topkar, V.V., Thapar, V., Wyvekens, N., Khayter, C., Iafrate, A.J., Le, L.P., Aryee, M.J., et al. (2015). GUIDE-seq enables genome-wide profiling of off-target cleavage by CRISPR-Cas nucleases. Nat Biotechnol *33*, 187-197. 10.1038/nbt.3117.
2. ImmunoMind Team (2019). immunarch: An R Package for Painless Bioinformatics Analysis of T-Cell and B-Cell Immune Repertoires. Zenodo. 10.5281/ZENODO.3367200.